FINAL REPORT
TURBINE RESEARCH PACKAGE FOR RESEARCH AND DEVELOPMENT OF HIGH PERFORMANCE AXIAL FLOW TURBINE-COMPRESSOR

written by

R. Cohen, W.K. Gilroy, F.D. Havens

approved by

P. Bolan

prepared for

NATIONAL AERONAUTICS AND SPACE ADMINISTRATION

CONTRACT NAS3-4179

Pratt & Whitney Aircraft

DIVISION OF UNITED AIRCRAFT CORPORATION

EAST HARTFORD, CONNECTICUT

NASA CR-54883
PWA-2822

FINAL REPORT
TURBINE RESEARCH PACKAGE FOR RESEARCH AND DEVELOPMENT OF HIGH PERFORMANCE AXIAL FLOW TURBINE-COMPRESSOR

Written by

R. Cohen, W. K. Gilroy, F. D. Havens

Approved by

P. Bolan

December 1966

Prepared for

NATIONAL AERONAUTICS AND SPACE ADMINISTRATION

CONTRACT NAS3-4179

Technical Management
NASA Lewis Research Center
Cleveland, Ohio
Space Power System Division

J. A. Heller

Fluid System Components Division
Consultant Harold E. Rohlik

Pratt & Whitney Aircraft
DIVISION OF UNITED AIRCRAFT CORPORATION

EAST HARTFORD, CONNECTICUT

#40

FOREWORD

This report was produced in accordance with NASA Contract NAS3-4179 under the technical management of J. A. Heller and consultation with H. E. Rohlik, NASA Lewis Research Center, Cleveland, Ohio. It describes the design and mechanical testing of the turbine research package produced in accordance with Article I, Section B of the contract.

TABLE OF CONTENTS

LIST OF FIGURES

LIST OF FIGURES (Continued)

LIST OF TABLES

I. SUMMARY

The turbine research package is a test rig intended to provide cold-flow aerodynamic performance data for the Brayton-cycle compressor drive turbine. This turbine is a single-stage axial-flow unit designed to provide a high efficiency potential.

The turbine research package was designed to provide a convenient mechanical configuration for aerodynamic testing. This unit was constructed and tested mechanically to twenty per cent above its design speed. It demonstrated satisfactory mechanical characteristics and completed the required acceptance test. The National Aeronautics and Space Administration plans to conduct aerodynamic testing at the Lewis Research Center. The turbine package was delivered to NASA on March 1, 1966.

II. INTRODUCTION

The NASA is conducting an evaluation program of candidate Brayton-cycle turbomachinery configurations. As a part of this program, Pratt & Whitney Aircraft has designed a turbine-compressor supported on gas bearings incorporating a six-stage axial-flow compressor driven by a single-stage axial-flow turbine. A turbine research package is provided to permit evaluation of the aerodynamic performance of the turbine using low-temperature gas. The turbine research package incorporates oil-lubricated rolling-contact bearings.

The turbine for the turbine-compressor is designed to provide high efficiency and reliability potential. The specific turbine design conditions for the turbine-compressor are as follows:

working fluid	argon	total pressure ratio	1.56
flow rate, lb/sec	0.611	operating life, hours	10,000
inlet total temperature, °R	1950	rotational speed, rpm	50,000
inlet total pressure, psia	13.20	maximum speed, rpm	60,000

The rotational speed was selected to provide low compressor aerodynamic losses, low bearing losses, and margin from critical speeds.

Since the turbine research package is a cold-flow rig, its operating conditions differ from those of the actual turbine so that an accurate aerodynamic simulation is achieved. Design conditions for the turbine research package are:

working fluid	argon	total pressure ratio	1.56
flow rate, lb/sec	1.184	rotational speed, rpm	25,800
inlet total temperature, °R	520	maximum speed, rpm	31,000
inlet total pressure, psia	13.20		

Particular design objectives included high mechanical integrity, versatility, and ease of assembly and disassembly. The package is capable of operating at speeds in excess of 120 per cent of design speed, at inlet temperatures as high as 710°R, and inlet pressures as high as 23 psia. The complete turbine research package is shown in Figures 1 and 2.

The discussion that follows begins by describing the design of the turbine for the turbine-compressor because of the dependence of the turbine research package design on the turbine-compressor turbine design. This is followed by a description of the turbine research package, and then by a presentation and discussion of the results of the mechanical testing.

III. TURBINE AERODYNAMIC DESIGN

The turbine blading for the axial-flow Brayton-cycle turbine-compressor was selected with the objective of producing high efficiency and high reliability potential. Preliminary study indicated that an efficient turbine could be designed for this application over a moderate range of speeds. Therefore, a rotational speed of 50,000 rpm was selected based on compressor design requirements*. With the compressor work, speed, and flow defined, the first major turbine design selections were the size or diameter of the turbine wheel and the number of stages. This choice was governed by the most significant turbine design variable, the velocity ratio, ν **. A high mean velocity ratio of 0.697 was selected to provide high efficiency potential. This resulted in a mean blade diameter of 4.1 inches for a single-stage turbine. Coupled with the high velocity ratio, high reaction was selected in the interest of high efficiency.

The Brayton cycle operates with low gas flow leading towards a design of low axial velocity, which has several advantages and disadvantages. A low axial velocity requires a long blade which minimizes tip clearance and end loss effects. Also, the kinetic energy of the gas leaving the turbine is lower and the exit diffuser losses are minimized. Therefore, low axial velocity provides the highest efficiency potential. The longer blades result in more gas turning at the blade root, and lower hub-tip diameter ratio which generally produces an airfoil with larger twist from root to tip. Also, the longer blades result in higher stresses. The blade stresses are not excessive over a moderate range of designs; therefore, low axial velocity was selected in an effort to achieve high efficiency.

The thermodynamic design parameters of the turbine are presented in Table 1. The predicted efficiencies are based on conservative loss coefficients which were adjusted by a 1/5 power law to account for the effects of low Reynolds number (the Reynolds number for both the nozzles and blades, based on the axial projection of the chord, is about 25,000). Gas leakage over the blade tips is estimated to be approximately 3 per cent of the primary flow. The predicted efficiencies indicate that the turbine work can be accomplished at a pressure ratio slightly smaller than originally specified.

---

* Final Report, Compressor Research Package for Research and Development of High Performance Axial-Flow Turbomachinery, PWA-2933, Contract NAS3-4179

**velocity ratio is defined as the ratio of the mean wheel linear speed, U, to the square root of twice the actual turbine work, Δh. $\nu = U/\sqrt{2\Delta h}$

TABLE 1

Brayton-Cycle Turbine-Compressor
Turbine Thermodynamic Design

stage work, Btu/lb	32.82
rotational speed, rpm	50,000
pressure ratio across turbine	
total to total	1.531
total to static	1.577
pressure ratio, flange to flange*	
total to total	1.545
total to static	1.556
velocity ratio (actual)	0.697
axial gas velocity to mean blade velocity ratio	0.387
exit axial Mach number	0.187
total-to-total efficiency	0.867
total-to-static efficiency	0.812
exit gas angle (mean), degrees	80.0
hub-tip diameter ratio	0.596
blade root static pressure ratio	1.11
flange-to-flange* total-to-total efficiency	0.842
flange-to-flange* total-to-static efficiency	0.833

The selected gas angles relative to the plane of rotation and thermodynamic conditions entering and leaving each airfoil row at root, mean and tip locations are presented in Table 2. This table lists conditions, averaged circumferentially, immediately forward of the leading edge, or immediately downstream of the trailing edge of the blades and vanes. The fluid conditions in Table 2 represent the mainstream except for the conditions under "Leaving Turbine". At this position complete mixing of the leakage with the mainstream flow is assumed.

The selected gas triangles practically provide free vortex flow. However, they are modified to provide a flow pattern which requires no radial flow shift due to compressibility effects as the gas passes through a blade row. The resulting flow pattern permits more airfoil passage convergence at the blade root and nozzle tip which provides higher efficiency potential.

* flange-to-flange is from scroll inlet flange to diffuser exit flange

TABLE 2

Brayton-Cycle Turbine-Compressor
Turbine Gas Triangles

Radial Station	Root	Mean	Tip
Entering Vane			
total temperature, °R	1950	1950	1950
total pressure, psfa	1882	1882	1882
static temperature, °R	1947	1936	1931
static pressure, psfa	1875	1851	1837
axial velocity C_x, fps	136.8	282.5	324
absolute swirl velocity C_{uo}, fps	0	0	0
gas inlet angle α_o, degrees	90.0	90.0	90.0
Leaving Vane			
static temperature, °R	1718	1811	1853
static pressure, psfa	1347	1539	1625
axial velocity C_x, fps	343.5	311.4	307
absolute swirl velocity C_{u1}, fps	1140	874	708
gas exit angle α_1, degrees	15.3	19.6	23.5
Reynolds number		2.53×10^4	
flow area, ft^2		0.0308	
Entering Blade			
relative total temperature, °R	1769	1823	1896
relative total pressure, psfa	1449	1566	1727
static temperature, °R	1711	1810	1855
static pressure, psfa	1334	1536	1635
axial velocity C_x, fps	322	292	288
relative swirl velocity W_{u2}, fps	506	-10	-416
wheel speed U_2, fps	668	895	1121
gas inlet angle β_2, degrees	32.4	92.0	145.4
Leaving Blade			
static pressure, psfa	1192	1193	1193
relative swirl velocity W_{u3}, fps	779	957	1192
wheel speed U_3, fps	668	895	1121
gas exit angle β_3, degrees	24.8	19.8	16.8
Reynolds number		2.56×10^4	
flow area, ft^2		0.0315	

TABLE 2 (Continued)

	Root	Mean	Tip
Leaving Turbine			
total temperature, °R		1686	
static temperature, °R	1666	1666	1666
total pressure, psfa		1229	
axial velocity C_{x3}, fps	348	346	355
absolute swirl velocity, C_{u3}, fps	81	61	46
absolute gas exit angle α_3, degrees	76.9	80.0	82.6

The nozzle vane geometry of the turbine-compressor is presented in Figure 4 and Table 3.

The airfoil contours were selected to form gas passages with high convergence and low diffusion rates in order to provide conservative velocity distributions. These velocity distributions at the root, mean and tip radial locations are presented in Figures 5, 6 and 7. The vanes are straight-line faired to determine intermediate airfoils.

The vanes operate at an average metal temperature of 1947° R and the stresses are very low in the turbine-compressor, as indicated in Table 3. The selection of PWA 655 material (equivalent to Inconel 713) for the vanes provides a very large design margin. At 1960°R, the nozzle material has a yield strength of 75,000 psi and a creep strength for 10,000 hours of 24,000 psi. The predicted bending stress in the vanes is only 224 psi.

TABLE 3

Turbine Vane Dimensions and Stresses

Radial Station	Root	Mean	Tip
number of vanes		30	
material		AMS 5382	
airfoil weight, lbs		0.012	
diameter, in	3.163	4.150	5.137
average radial height, in		1.021	
pitch, in	0.331	0.435	0.538
axial width, in	0.419	0.500	0.581
vane chord, in	0.622	0.705	0.797
solidity	1.880	1.622	1.481
gas bending stress, psi	0	224	0
total axial thrust, lbs		27.5	
total tangential load, lbs		16.6	

The blade geometry at root, mean, and tip radial locations in the turbine of the turbine-compressor is presented in Figure 8 and Table 4. The solidity of each radial station was selected to provide minimum losses. As in the nozzle design, airfoil contours were selected at these three radial stations to provide conservative velocity distributions. Figures 9 and 10 present the velocity distributions of the blade root and mean sections. At the blade tip sections, the wide spacing between airfoils prevented the application of two-dimensional channel analysis to determine the velocity distributions. The tip airfoil was selected on the basis of experimental data for similar sections in order to produce low-loss flow.

Initially, straight-line fairing from the root section to the mean section and from the mean section to the tip was examined. This geometry did not produce satisfactory intermediate airfoils and curve-line fairing was employed. The axial projection of the blade retained a straight leading edge and trailing edge from root to mean and mean to tip, as shown in the blade elevation, Figure 11. In the turbine-compressor, the centrifugal stress due to the airfoil pull, which is presented in Table 4, represents the primary blade stress. The gas bending stresses are very small. While the centers of gravity of the root, mean, and tip sections are located on a radial line, the center of gravity of all sections could not be stacked on a radial line. As a result, some centrifugal bending stresses are introduced. Figure 12 presents the gas bending and the centrifugal bending stresses superimposed on the blade pull centrifugal stress. Also included in Figure 12 are the allowable 0.1, 0.2 and 1.0 per cent creep stresses for 10,000 hours for the nickel-base turbine material, PWA 1007. The blade stress levels are conservative and the blade is designed with ample design margin.

TABLE 4

Turbine Blade Dimensions and Stresses

Radial Station	Root	Mean	Tip
number of blades		26	
material		PWA 1007	
diameter, in	3.063	4.10	5.137
average radial height, in		1.037	
pitch, in	0.370	0.494	0.620
axial width, in	0.701	0.500	0.298
blade chord, in	0.732	0.724	0.725
solidity	1.980	1.464	1.167
centrifugal stress, psi	23,350	20,160	0
gas bending stress, psi	307	389	0
airfoil metal temperature, °R	1760	1821	1855
total axial thrust, lbs		30.9	
total tangential loads, lbs		17.92	

A photograph of the turbine rotor with integrally-machined blades is presented in Figure 13. This design exhibits a fairly large twist along the leading edge which is necessary to provide proper alignment of the airfoil with the gas flow (essentially zero incidence). This blading design is predicted to be satisfactory. However, as a result of consultation with the NASA, an effort was made to remove this twist. An airfoil was faired by hand retaining the root, mean and tip airfoils. The hand fairing resulted in somewhat less twist and reduced centrifugal bending stresses which are shown in Figure 14. However, the hand blending also resulted in high positive incidence in the outer half of the airfoil. Since airfoils with nearly zero incidence are required to provide low losses, the hand-blended configuration was not considered further.

A revised turbine airfoil fairing was developed in which the straight-line axial projection of the leading edge was changed to a curved line as shown in the blade elevation, Figure 15. The root, mean, and tip airfoil sections were retained except for a very small modification to the leading edge at the mean section. The incidence with this fairing was satisfactory and the apparent leading edge twist was reduced as illustrated by Figure 16. However, the centrifugal bending stresses in the turbine-compressor, Figure 17, were increased significantly and between 1 and 2 per cent creep is predicted locally at the leading edge in 10,000 hours. Since this stress is only local, the Number 2 blade design is predicted to be satisfactory.

The geometry of the turbine inlet scroll and duct is presented in Figure 18. The velocities in the duct are low (maximum velocity of 360 ft/sec for conditions in the turbine-compressor) to provide minimum losses. The transition ducting from the turbine exit to the inlet of the alternator drive turbine is shown in Figure 19. Since the alternator drive turbine is larger than the compressor drive turbine, an overall increase in flow area is required. The duct is designed to diffuse at a rate consistent with a 4-degree half-angle conical diffuser. Since the velocities are low in the ducting and since the first nozzle of the alternator drive turbine has high reaction, the transition duct should provide good flow conditions in the turboalternator.

The predicted total-to-total efficiency of the turbine as a function of velocity ratio is presented in Figure 20, and the flow parameter is presented in Figure 21 as a function of pressure ratio. These predictions are based on operation with design turbine inlet pressure and temperature. At significantly lower pressures, Reynolds number effects would be expected to change the predicted performance.

IV. DESCRIPTION OF TURBINE RESEARCH PACKAGE

The turbine research package is designed to provide a convenient means of evaluating the aerodynamic performance of the turbine-compressor turbine using low-temperature gas. A cross-sectional drawing of the turbine research package is presented in Figure 22 and photographs are presented in Figures 1 and 2. The argon enters through the inlet scroll and ducting (shown in Figure 23) to the turbine nozzle (Figure 24). The inlet scroll is reversed compared to the scroll designed for the turbine-compressor to permit instrumentation access. The argon then flows through the rotor and exhausts through the exit diffuser (Figure 25). Either the Number 1 turbine rotor, Figure 13, or the Number 2 turbine rotor, Figure 16, can be used. The turbine blades are integrally machined on the disk which is bolted to the shaft assembly (Figure 26). The shaft is supported by a roller bearing and a ball bearing which are jet-oil lubricated. The bearing compartment is sealed by a carbon face seal on the turbine end and a labyrinth seal on the drive end (Figure 27). The main bearing housing is shown in Figures 28 and 29 and includes a breather fitting as well as oil inlet and scavenge ports.

Both the roller bearing and the ball bearing (Figures 30 and 31) have an inner diameter of 20 millimeters and an outer diameter of 42 millimeters. The bearings are made of AMS-6444 steel and have silver-plated steel cages. Each bearing is cooled and lubricated by MIL-L-7808 lubricant or by an appropriate oil with similar characteristics at the operating conditions. A thermal map is presented in Figure 32 showing the predicted operating temperatures in the bearing area with an argon inlet temperature of 200°F and an oil inlet temperature of 80°F. Three iron-constantan thermocouples are located in the housing of each bearing to monitor bearing outer-race temperatures. Oil is metered to the bearings through 0.039-inch diameter orifices which results in an oil flow rate of 1.0 lb/min for each bearing. Bearing oil compartment design parameters are presented below:

oil supply pressure, psia	35
bearing compartment pressure, psia	6.0
rear labyrinth seal	
radial clearance, inch	0.010
leakage flow, lb/sec of air	0.006

The DN factor for the bearings (bearing inner diameter times design speed) in the turbine research package is 516,000 mm-rpm, which represents an adequate design for this application. With the maximum mechanical unbalance, design thrust, and operation at 31,000 rpm, the B-10* fatigue life of the ball bearing

*The B-10 life is the time required to fail 10 per cent of the bearings of a given type in a given application

is 1,320 hours. The roller bearing life at similar conditions is a little larger. Therefore, ample life is provided in the bearing designs.

The interface between the argon and the bearing compartment is sealed by a carbon face seal (Figure 33) which is held in contact with a rotating sealplate by a spring. An O-ring serves as the static secondary seal. The bearing compartment pressure should not be set below 2 psia to avoid oil foaming. Whenever practical, the bearing compartment pressure should be approximately equal to turbine discharge pressure to reduce the pressure drop across the carbon face seal. The bearing compartment breather pipes should be connected to the exhaust piping in order to provide bearing compartment pressures near the recommended values. The oil should be supplied at a pressure between 29 and 35 psi above the bearing compartment pressure. The other end of the shaft is sealed with a four-lip staggered labyrinth seal. The labyrinth seal was selected for use at this location to reduce the parasitic power consumption.

The heat loss rates from the gas path during operation without rig insulation were determined for an inlet temperature of 200°F and an inlet pressure of 13.2 psia. These values are presented below:

	Heat Loss Rate (Btu/hr)
inlet	670
scroll to turbine	156
case	50
oil	75
total loss	952 Btu/hr

These values do not include the heat generated in the bearings and seals which is carried away by the oil. The "oil" entry indicates that 75 Btu/hr is transferred from the gas path to the oil during operation. The total heat loss during operation without insulation represents about 2.1 per cent of the turbine output power, and therefore, will significantly affect the measured turbine efficiency. Consequently, operation with rig insulation is recommended.

The static structural and rotating parts are conservatively designed and have ample design margins. The lowest rotor critical speed is a rigid body mode which is dependent upon bearing springrate. As shaft speed or bearing load increase, the bearing springrate increases, and the rigid body critical speed increases. Figure 34 shows that for the minimum estimated springrate the rigid-body critical speed is 40,000 rpm at the maximum operating speed of 31,000 rpm. The first and second bending criticals are calculated to be at 55,000 and 93,000 rpm respectively, as shown on Figure 34.

The turbine research package employs the same airfoil and wall contours as are provided in the turbine-compressor package. Since the turbine research package operates with relatively low-temperature gas and at low speed, the stresses in the turbine research package are at acceptable levels at all operating conditions. The rotor is constructed of AMS 5660 and the most critical rotor stresses are in the shaft-disc attachment area. Table 5 presents these stresses at the worst anticipated conditions. Evidently adequate design margin is provided.

TABLE 5

Shaft - Disk Attachment Stresses
36,000 rpm
120°F ΔT (Disk to Shaft)
Maximum Tight Assembly Fit

Location	Maximum Stress	0.2% Yield Stress
disk snap	44,000 psi (shear) 73,000 psi (bending)	56,000 psi 99,000 psi
shaft flange	42,000 psi (hoop)	99,000 psi
shaft	45,000 psi (bending)	99,000 psi

The turbine rotor design has been analyzed to determine the consequences of overspeed operation. As rotating speed is increased, the disk snap area will yield first but fracture is predicted above 90,000 rpm. Therefore, ample design margin is provided. A summary of the overspeed characteristics is presented in Table 6.

TABLE 6

Turbine Overspeed Characteristics

Speed (rpm)	Failure Mode
49,000	disk snap yield
80,000	disk yield
94,000	disk snap fracture
97,000	disk burst

The turbine research package is provided with the instrumentation presented in Table 7 to permit evaluation of the aerodynamic performance of the turbine.

TABLE 7

Aerodynamic Instrumentation

Location	Static Pressure Taps	Other Provisions
scroll inlet	four	four 5/16-in. diameter holes for fixed probes
scroll radial section	ten taps spaced at one and one-half inch intervals in two rows approximately 180° apart	
upstream of nozzle	four in the inner wall and four in the outer wall	
downstream of nozzle	four in cavity forward of turbine rotor and four in outer wall	
exit diffuser	sixteen taps spaced at two-inch intervals in two rows approximately 180° apart	
diffuser exit	four in inner wall and four in outer wall	one radial traverse boss

Measurements of various clearances in the turbine research package are included in Appendix 1.

V. TEST PROGRAM

A. Introduction

The aerodynamic testing of the Brayton-cycle turbine-compressor turbine is planned to be conducted at the Lewis Research Center. No aerodynamic tests were conducted at Pratt & Whitney Aircraft. A test program was conducted to verify satisfactory mechanical operation of the turbine research package. These tests were conducted in two phases. First, the rotor dynamic performance was evaluated to ensure proper rotor behavior. Then the research package was subjected to an acceptance test to demonstrate satisfactory mechanical characteristics. The acceptance test required running the turbine at the design speed of 25,800 rpm for thirty minutes and at 120 per cent of design speed for ten minutes.

B. Test Facility

The test stand used for testing the turbine research package is shown in Figure 35. The test was controlled remotely from the control room shown in Figure 36. Air was supplied to the turbine inlet through pressure reduction and control valves. Drive air from the turbine was exhausted directly to the ambient environment. The oil lubrication system consisted of motor-driven supply and scavenge pumps, a reservoir, strainer and filter, and a control valve. The bearing compartment was vented to the ambient environment.

Vibration pickups (Consolidated Electrodynamics Corporation Type 4-H8-0001) were used to measure the vibration of the static cases at the drive end of the main bearing housing and at the turbine rotor shroud. Measurements were made for vibration in both the horizontal and vertical directions. Signals from the pickups were read on meters designed by Pratt & Whitney Aircraft and capable of measuring vibrations with amplitudes up to 0.0025 inch.

Rotor speed was sensed by two Electro-Products Laboratories Model 3016 magnetic speed pickups. The outputs of the pickups were read on two Dynapar Company Dynacounters.

Temperatures of the bearings and the lubricating oil at the inlet and outlet were sensed by thermocouples, with the thermocouple output being read on Brown potentiometers.

C. Rotor Dynamic Test

The dynamic operating characteristics of the rotor were measured to ensure proper mechanical operation of the turbine research package. The radial motion

of the disk was sensed by eddy-current-type proximity probes (Bentley Model 11-3-021-4). The probes were positioned 90 degrees apart (as shown in Figure 37) and were connected to the x and y axes of an oscilloscope to display the shaft orbit. Another proximity probe was used to measure the radial motion of the six-tooth speed pickup gear at the other end of the shaft.

To check proper mechanical operation of the turbine research package with the alternate turbine wheel and the coupling installed, pairs of proximity probes were mounted at either end of the coupling (as shown in Figures 38, 39 and 40) in addition to the probes described above. Testing was conducted at 2180; 15,180; 18,060; and 26,260 rpm. Figures 41, 42 and 43 show the test results at the turbine disk, the turbine end of the coupling and the gearbox end of the coupling. The orbits shown at 2180 rpm are the result of radial play in the roller bearing and runout of the rotating member being viewed by the probes. Subtracting the orbit diameter at 2180 rpm from the orbit diameter at 26,260 rpm on Figure 41 results in a dynamic shaft movement of 0.006 inch double amplitude at the turbine disk. Figure 42 indicates a dynamic motion of 0.002 inch double amplitude at the turbine end of the coupling, and Figure 43 shows negligible dynamic motion at the gearbox end of the coupling. Maximum case vibration of 0.00025 inch was recorded in the vertical plane at the drive end of the main bearing housing at 26,260 rpm.

Prior to the acceptance test using the reference turbine wheel, a rotor dynamics check was made without the coupling installed. Data at 10,000; 15,000; 20,000; 26,000; and 31,150 rpm is shown on Figures 44, 45, and 46. Maximum case vibration of 0.0001 inch occurred in the vertical plane at the drive end of the main bearing housing at 31,150 rpm. Figure 46 shows that the rotor displacement was 0.005 inch double amplitude at the turbine disk and 0.002 inch at the drive end at 31,150 rpm.

The test results indicate that rotor dynamic behavior is satisfactory.

D. Acceptance Test

An acceptance test of the turbine research package to demonstrate the mechanical integrity of the unit was required. The specified acceptance test consisted of acceleration to design speed for 30 minutes, acceleration to 120 per cent of design speed (31,000 rpm) and operation at this speed for 10 minutes, and deceleration. The test was specified as a free spinup, and, therefore, no load was applied to the shaft.

The acceptance test was successfully completed on February 23, 1966. The vibration pickups indicated a maximum motion of 0.0001 inch. This value

was measured in the horizontal plane at the turbine rotor shroud. Maximum ball and roller temperatures were 157 and 117°F, respectively. These measurements were substantially in agreement with the data recorded during the rotor dynamic test.

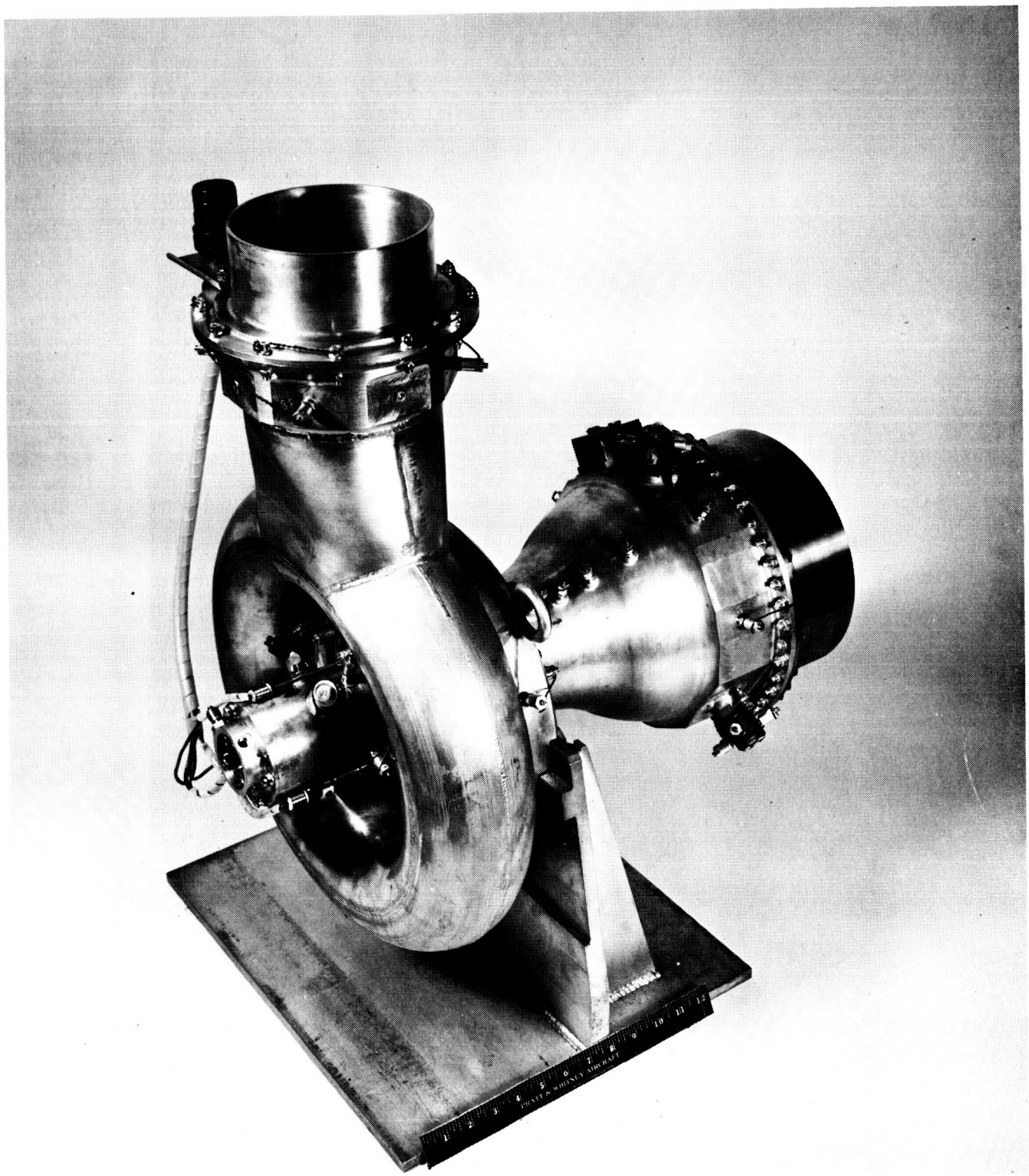

Figure 1 Gas Inlet End of Turbine Research Package XP-62534

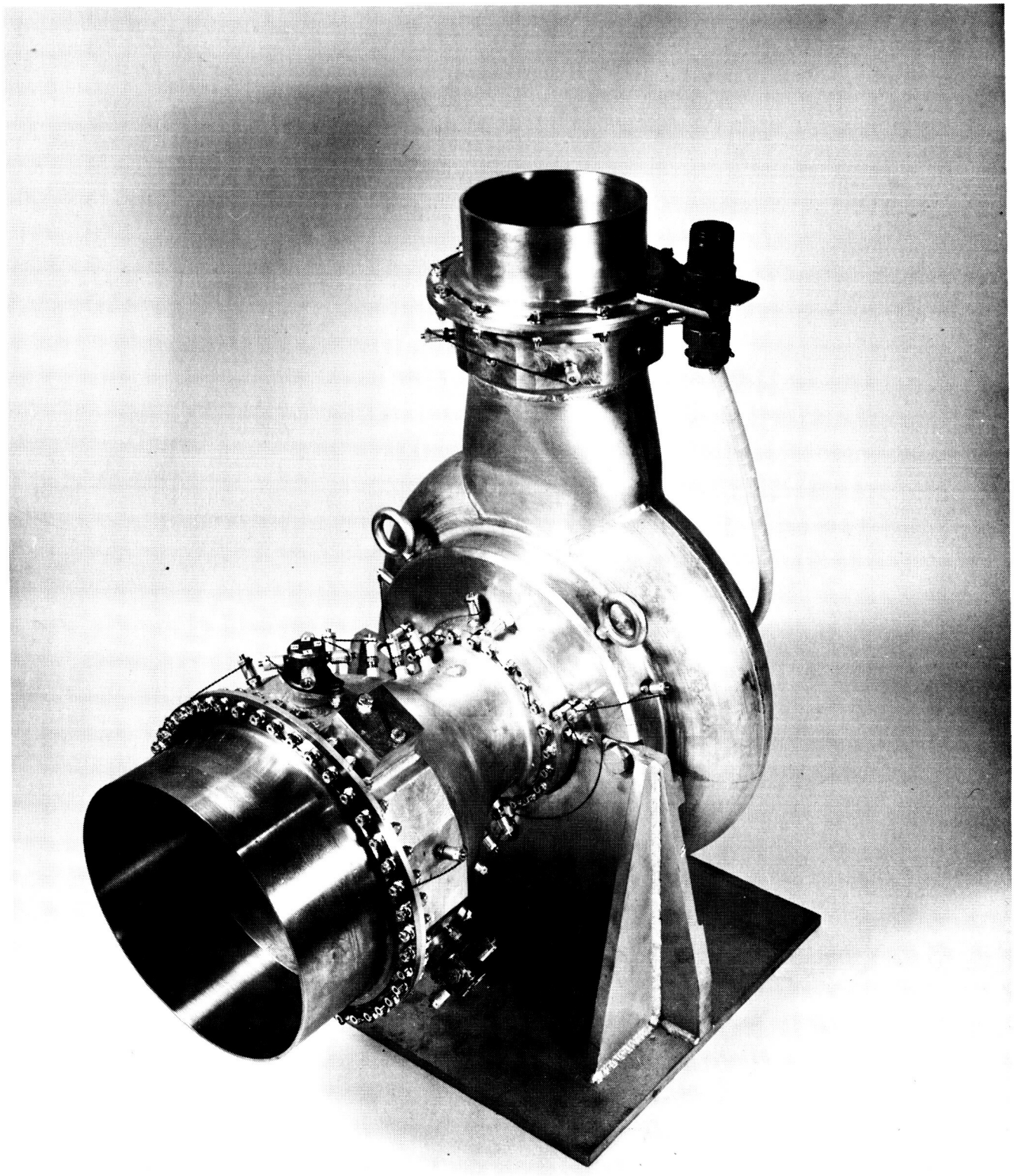

Figure 2 Gas Exhaust End of Turbine Research Package XP-62533

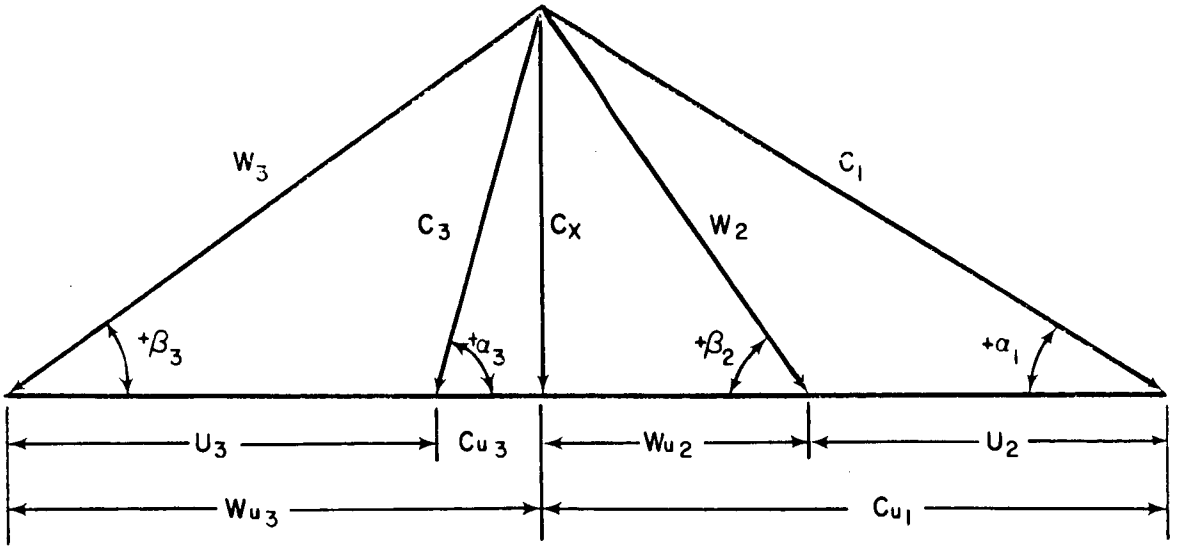

C - ABSOLUTE GAS VELOCITY, FT/SEC
U - BLADE VELOCITY, FT/SEC
W - RELATIVE GAS VELOCITY, FT/SEC
α - ABSOLUTE GAS ANGLE MEASURED FROM PLANE OF ROTATION
β - RELATIVE GAS ANGLE MEASURED FROM PLANE OF ROTATION

SUBSCRIPTS

1 - STATION AT NOZZLE TRAILING EDGE
2 - STATION AT ROTOR LEADING EDGE
3 - STATION AT ROTOR TRAILING EDGE
X - AXIAL

Figure 3 Turbine Velocity Triangle Nomenclature

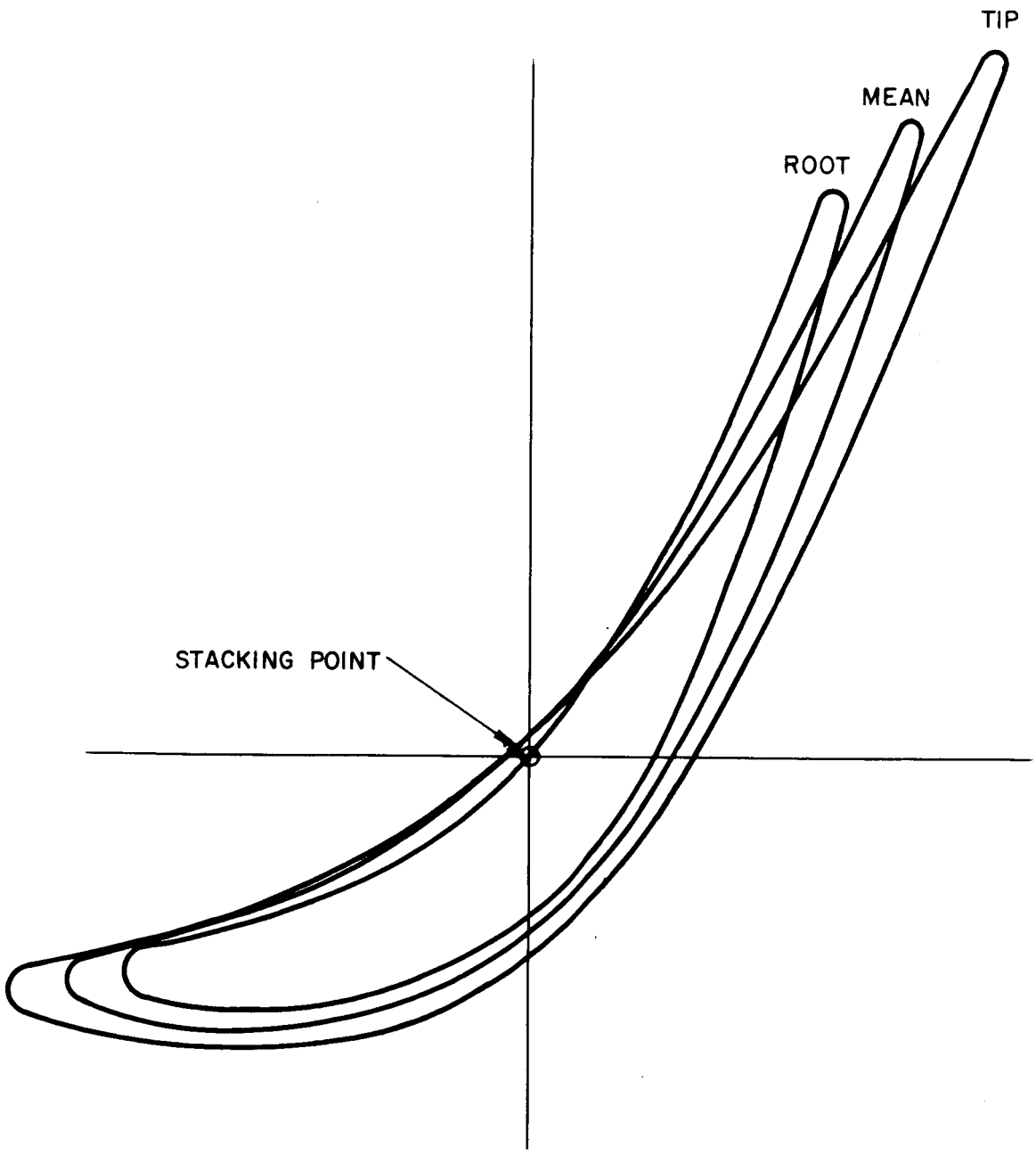

Figure 4 Turbine Vane Airfoil Geometry

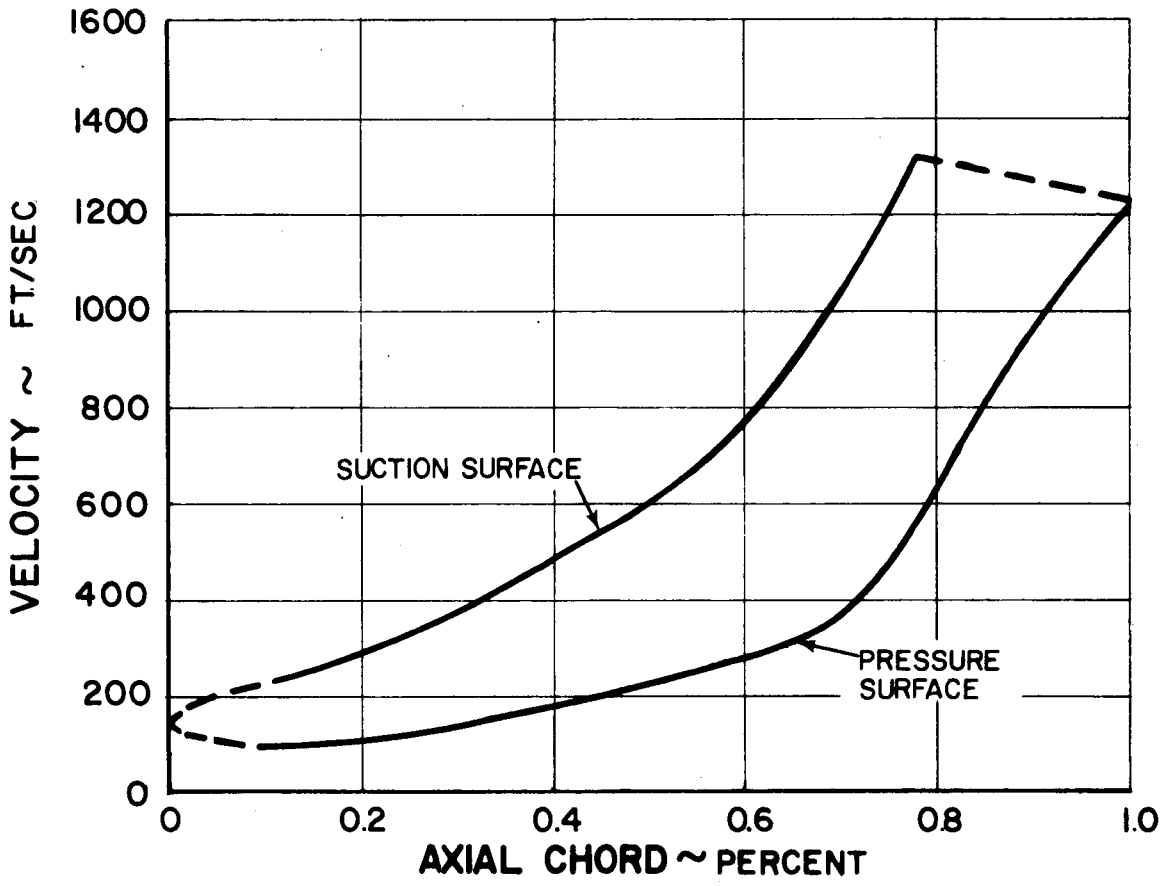

Figure 5 Velocity Distribution at Turbine-Compressor Root Section of Vane

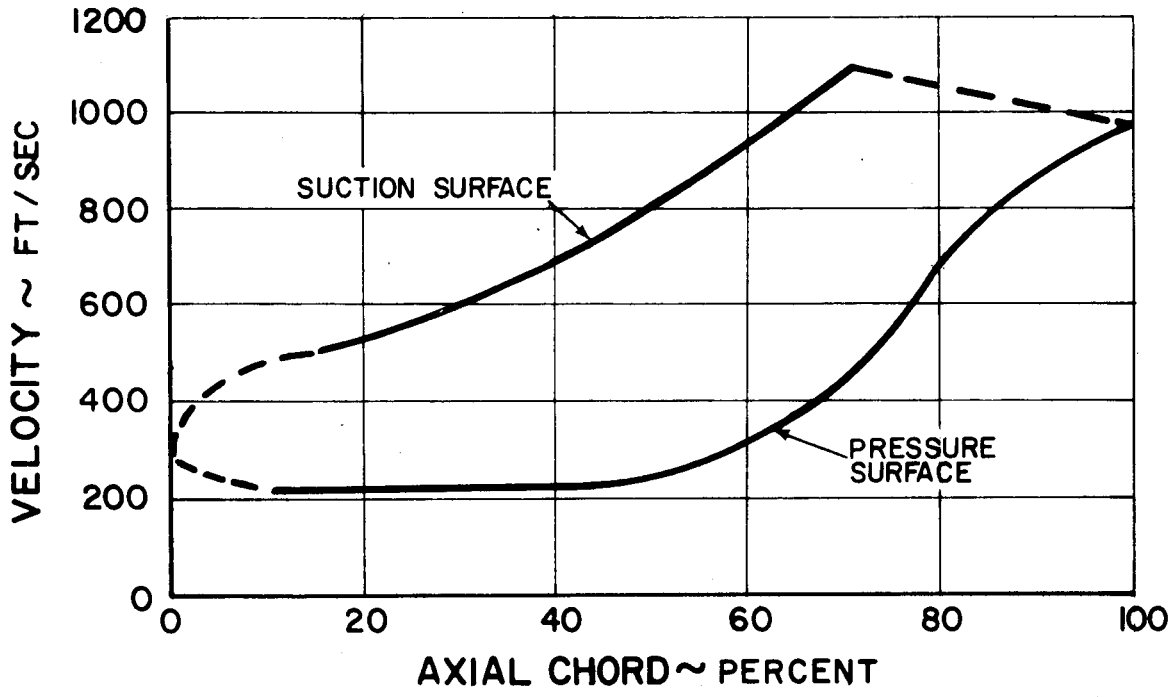

Figure 6 Velocity Distribution at Turbine-Compressor Mean Section of Vane

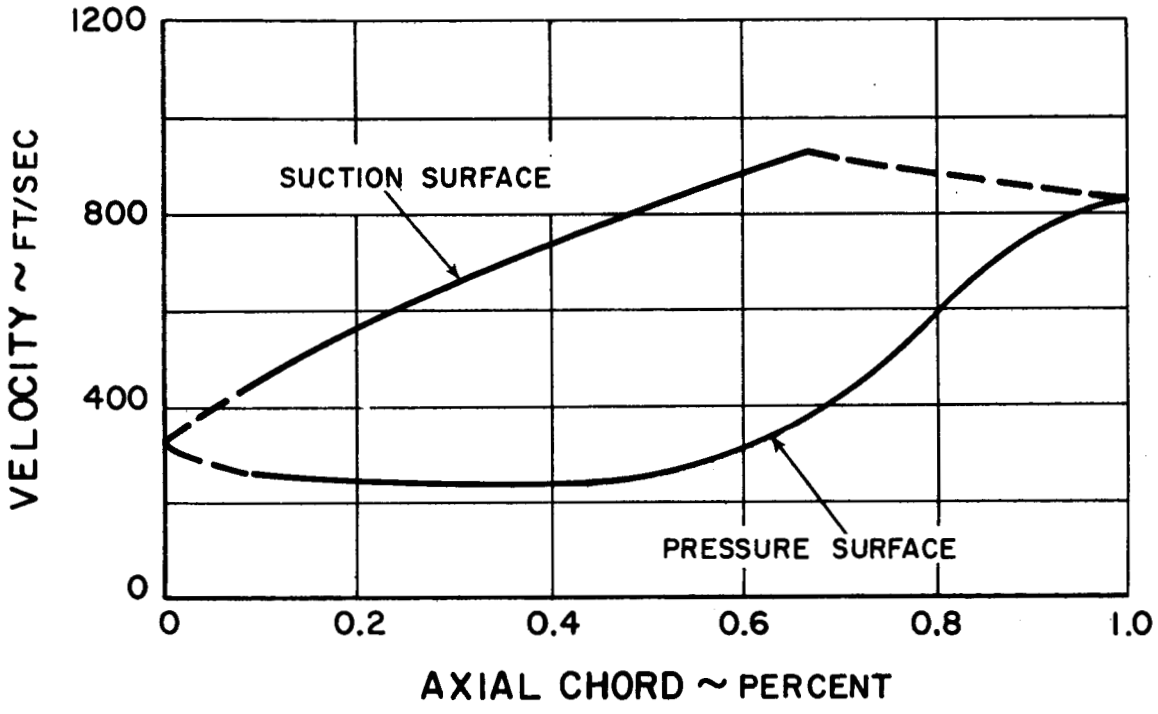

Figure 7 Velocity Distribution at Turbine-Compressor Tip Section of Vane

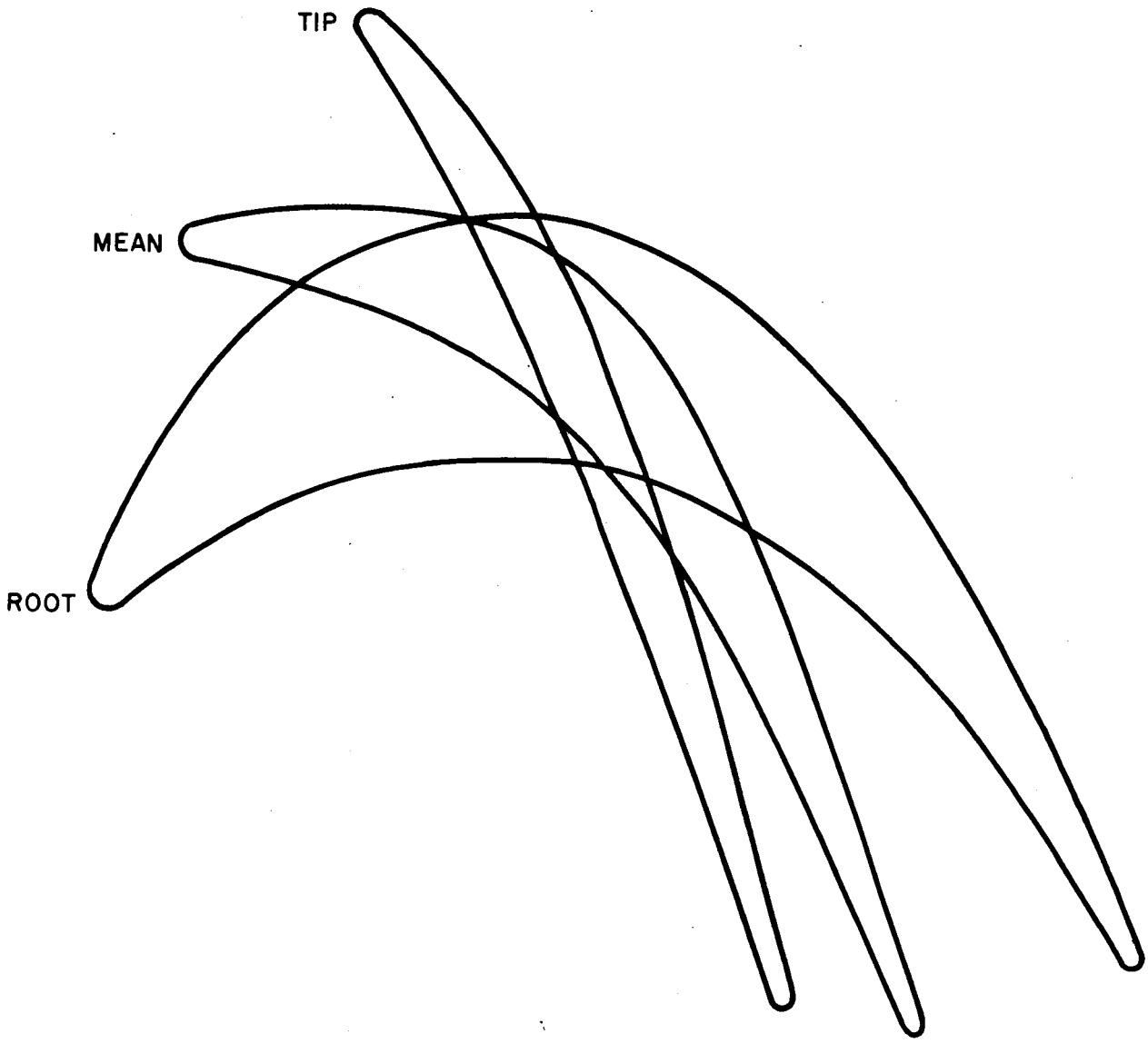

Figure 8 Turbine Blade Airfoil Geometry

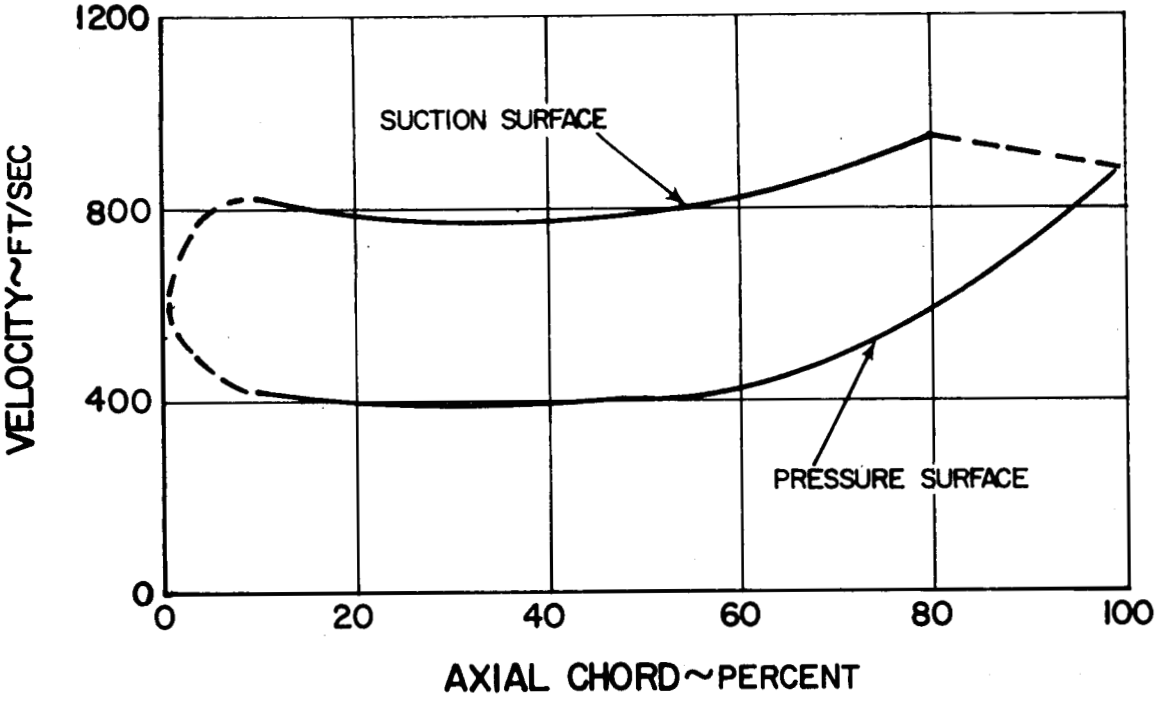

Figure 9 Velocity Distribution at Turbine-Compressor Root Section of Blade

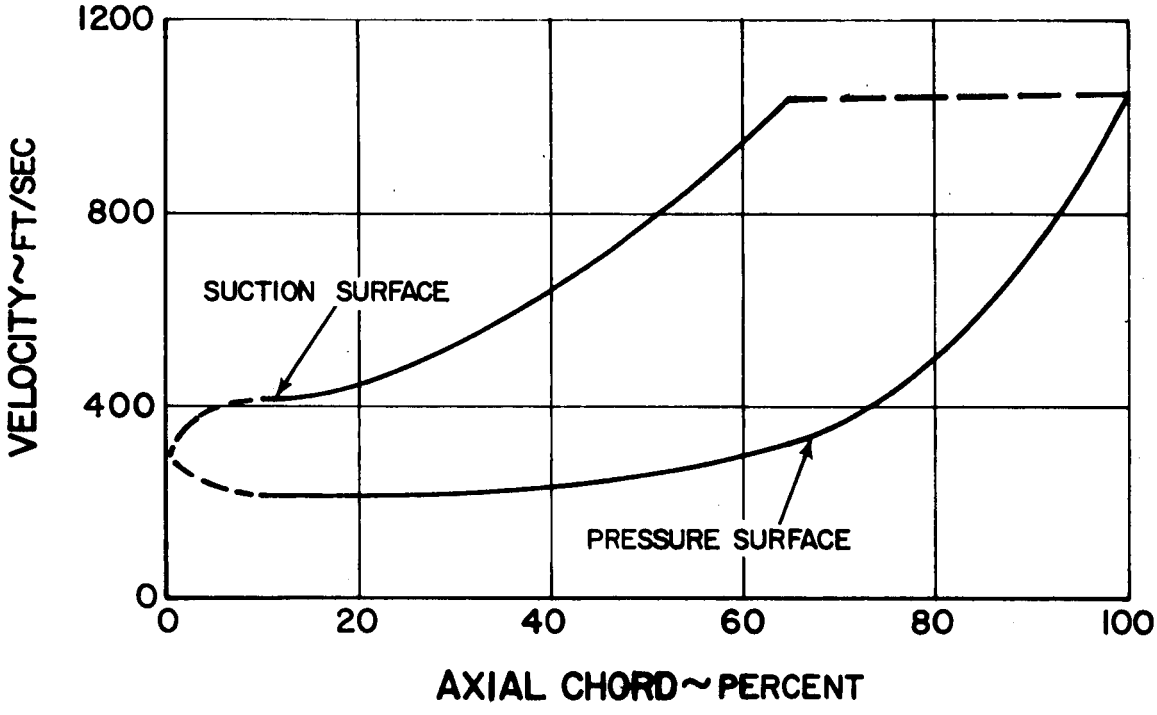

Figure 10 Velocity Distribution at Turbine-Compressor Mean Section of Blade

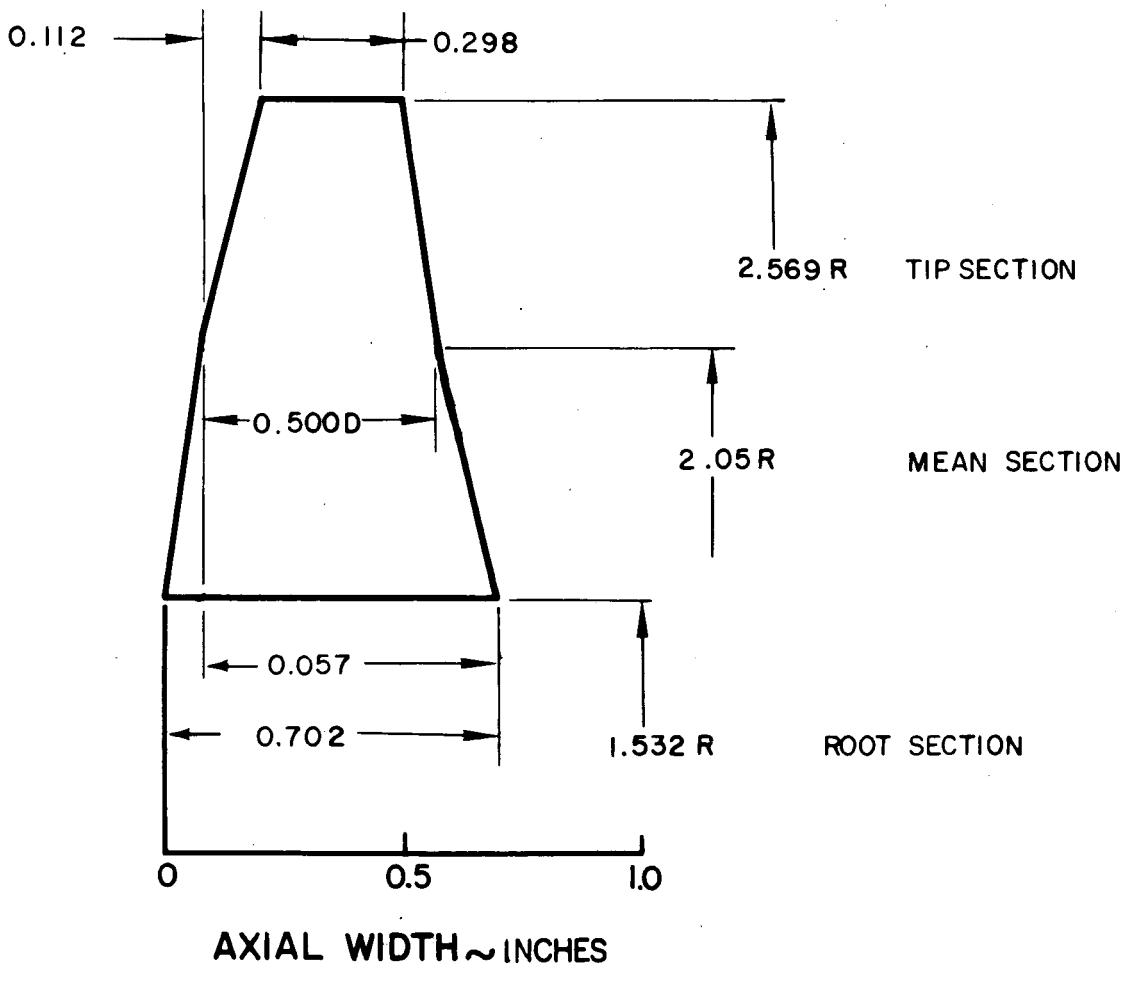

Figure 11 Number 1 Blade Fairing. Blade Elevation (All Dimensions Hot)

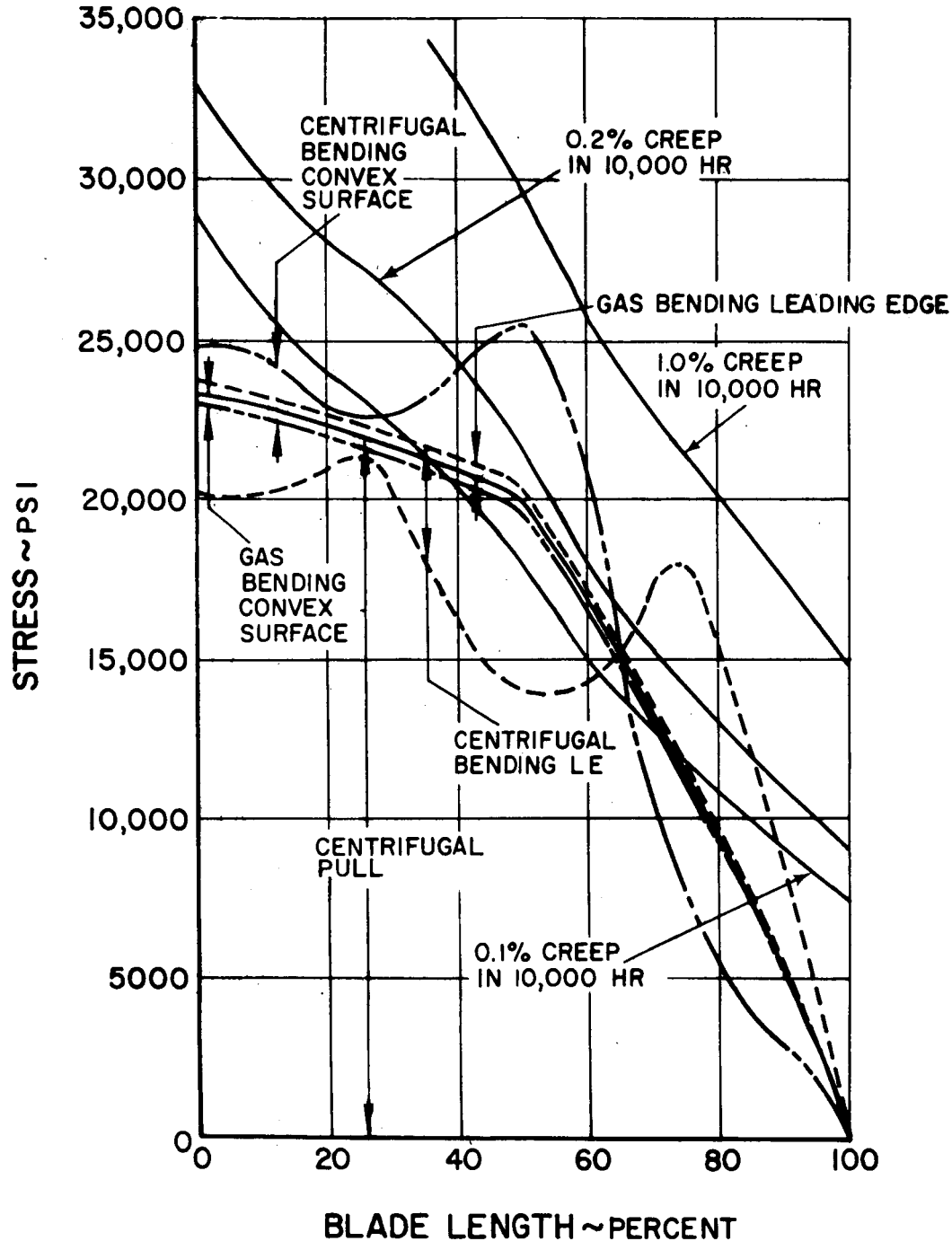

Figure 12 Number 1 Blade Fairing. Turbine-Compressor Blade Stress vs Per Cent Length at 50, 000 rpm

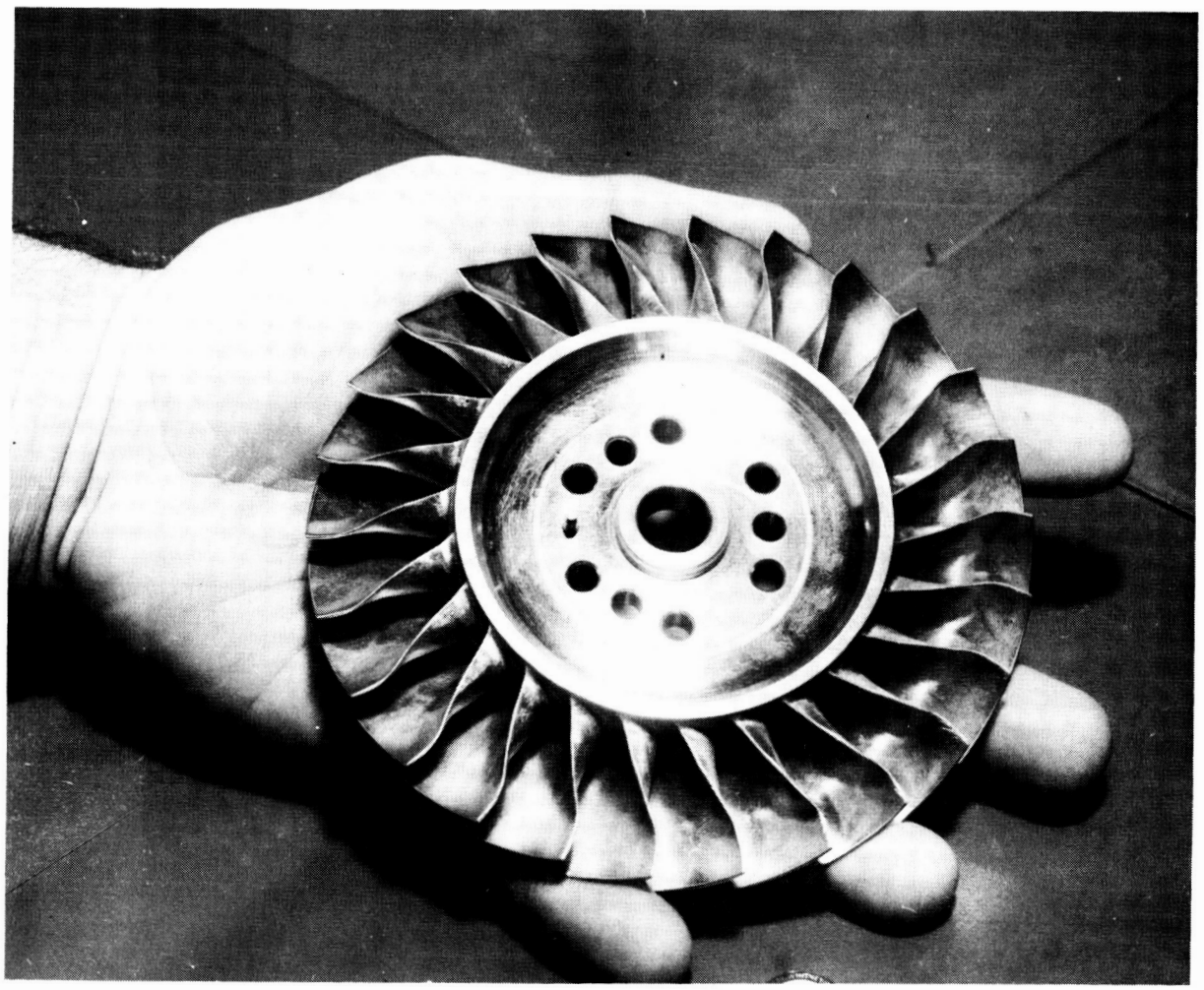

Figure 13 Number 1 Turbine Rotor X-20381

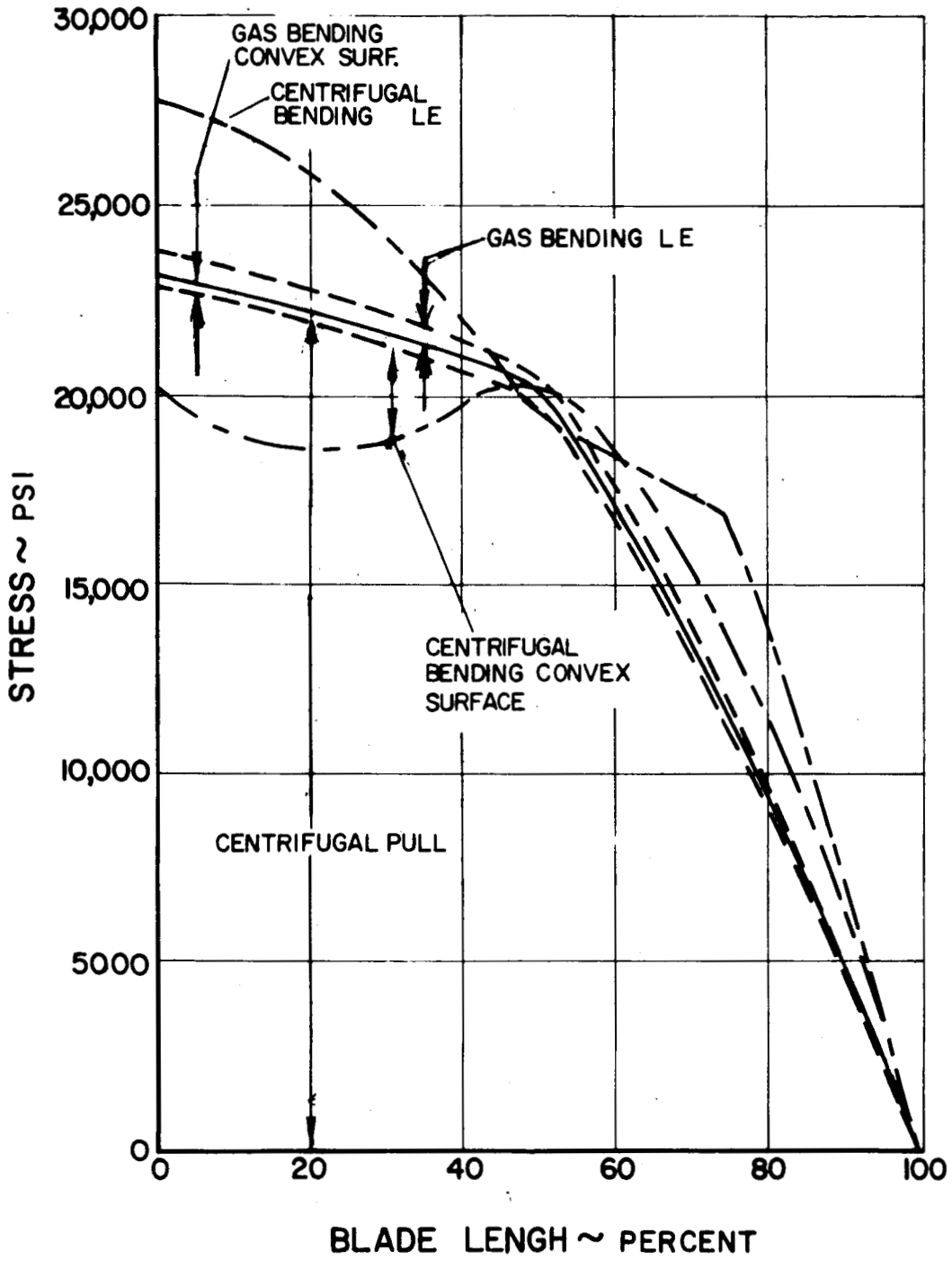

Figure 14 Hand-Blended Airfoil. Turbine-Compressor Blade Stress vs Per Cent Length at 50, 000 rpm

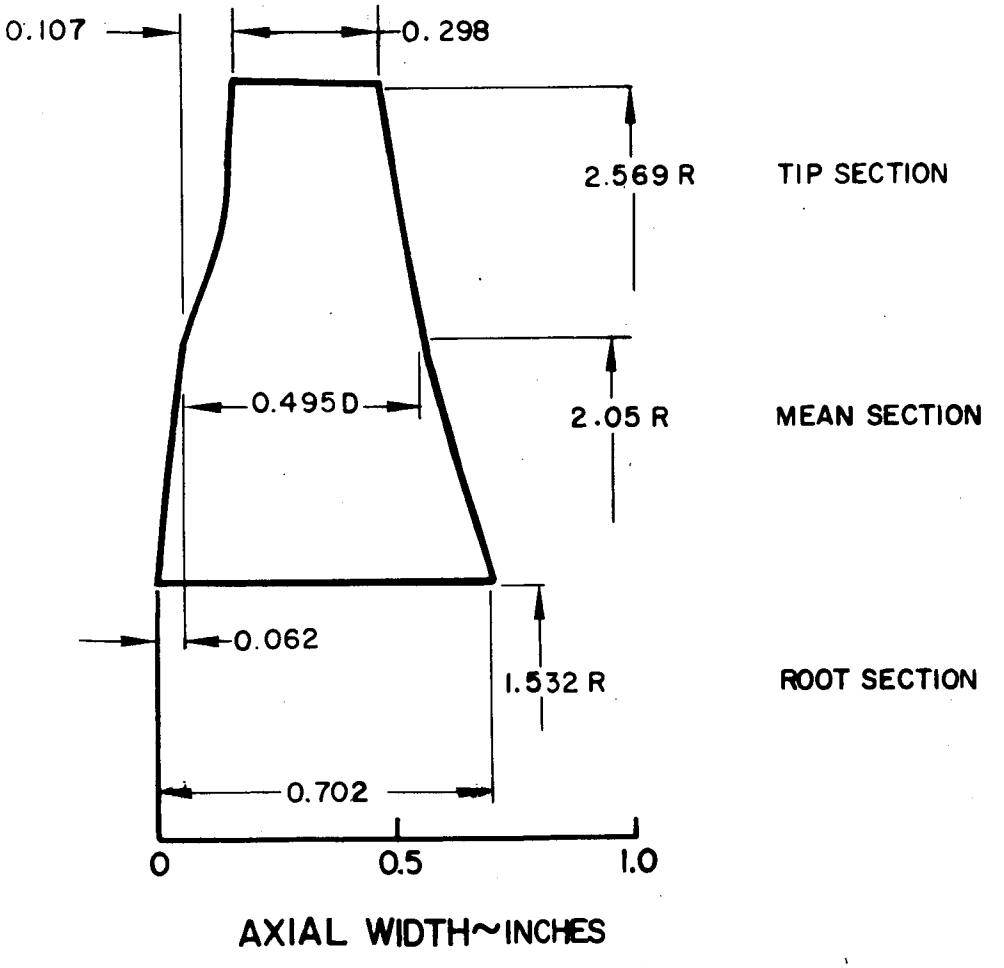

Figure 15 Number 2 Blade Fairing. Blade Elevation (All Dimensions Hot)

Figure 16 Number 2 Turbine Rotor M-37156

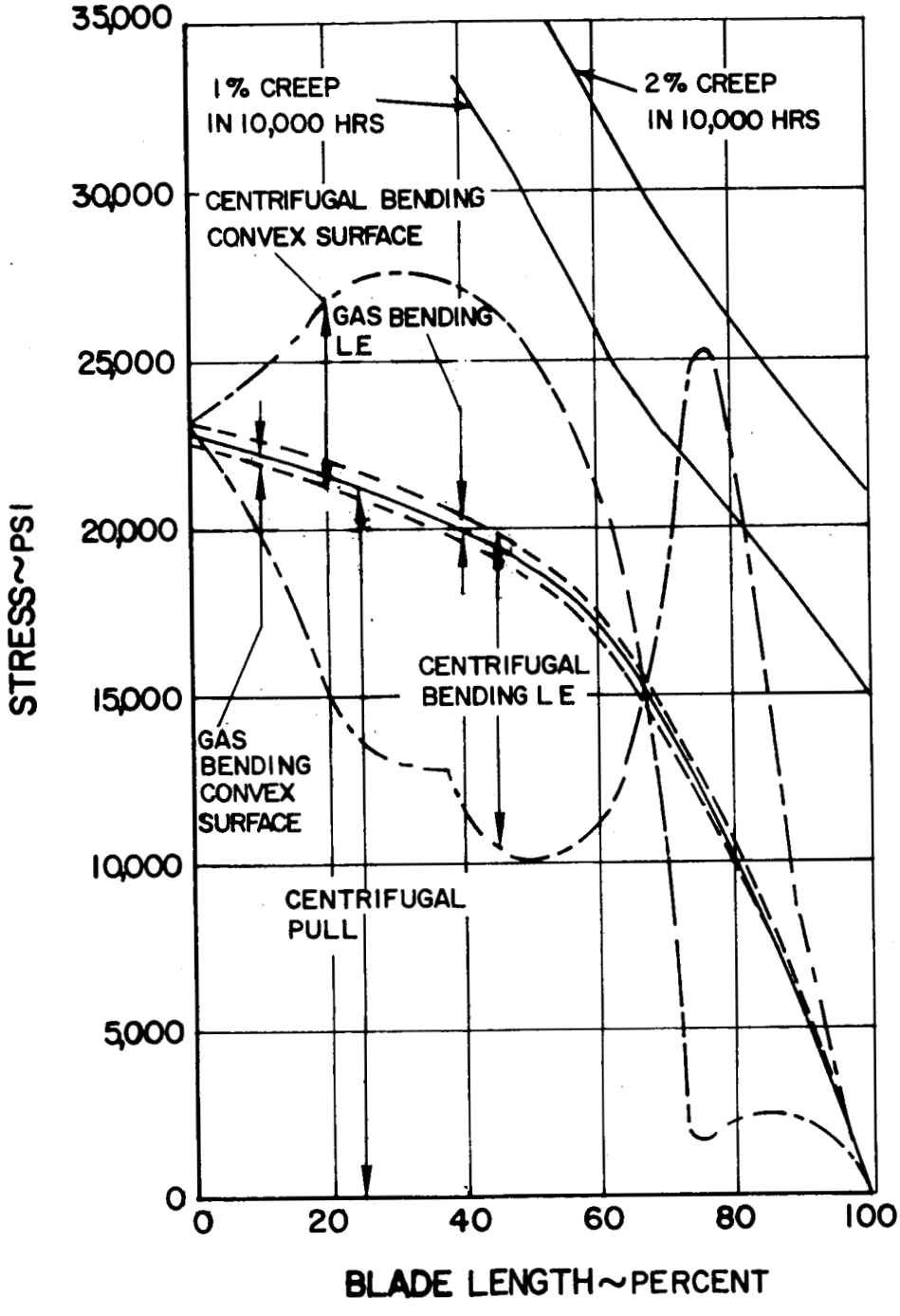

Figure 17 Number 2 Blade Fairing. Turbine-Compressor Blade Stress vs Per Cent Length at 50, 000 rpm

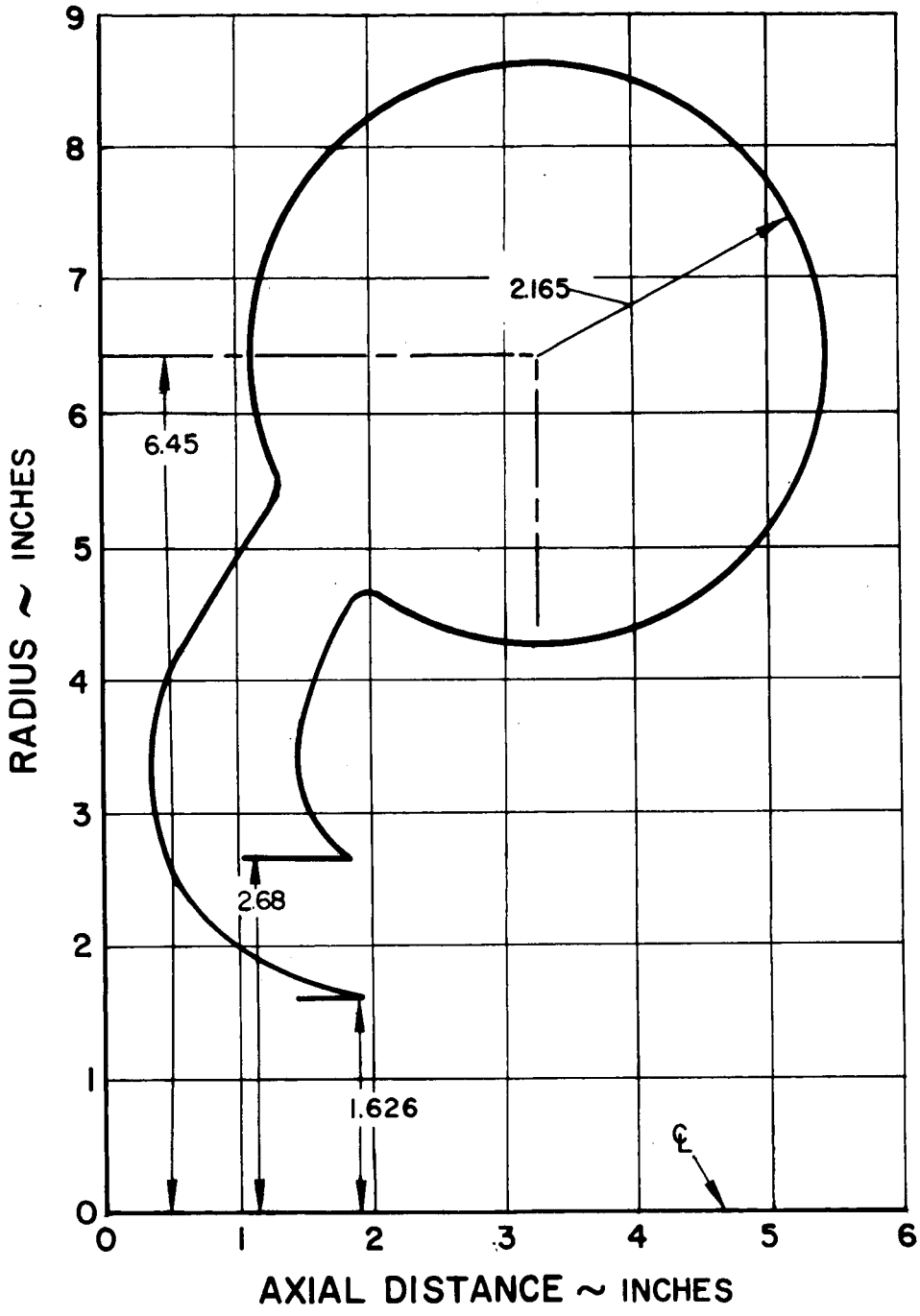

Figure 18 Turbine Inlet Duct

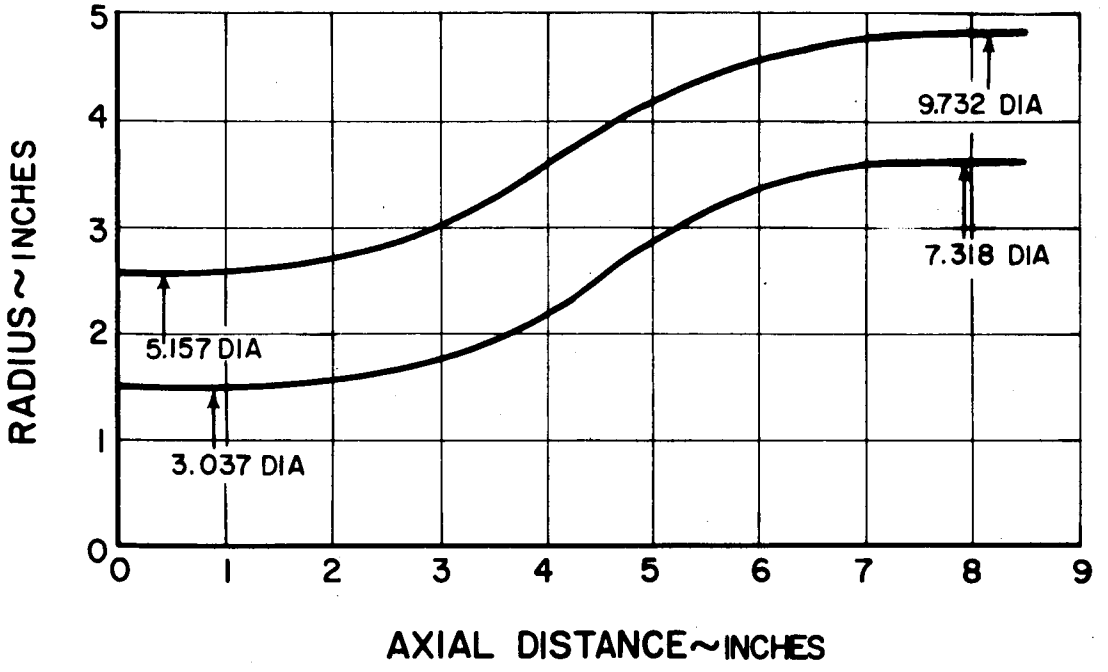

Figure 19 Exit Diffuser

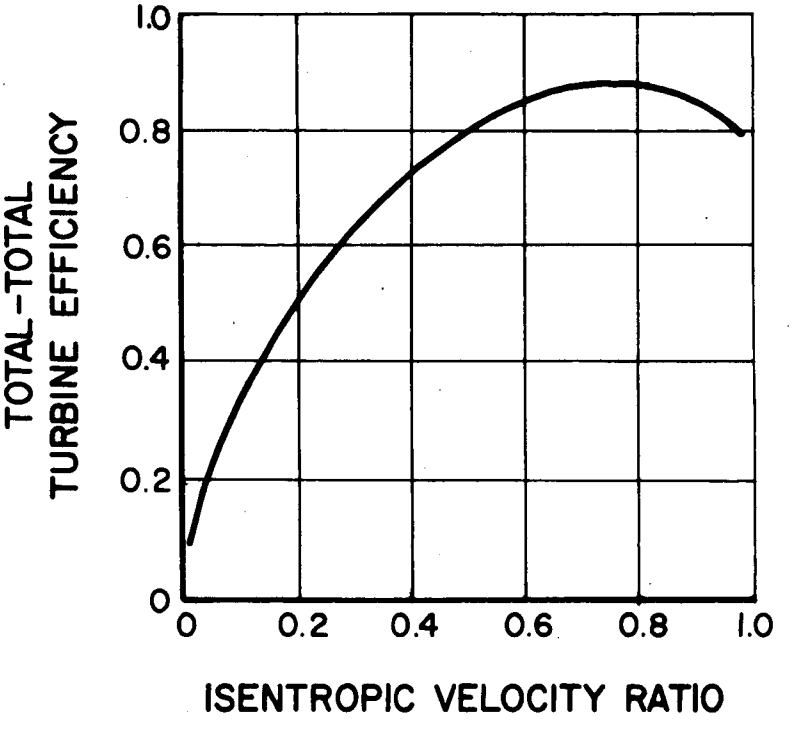

Figure 20 Estimated Off-Design Performance

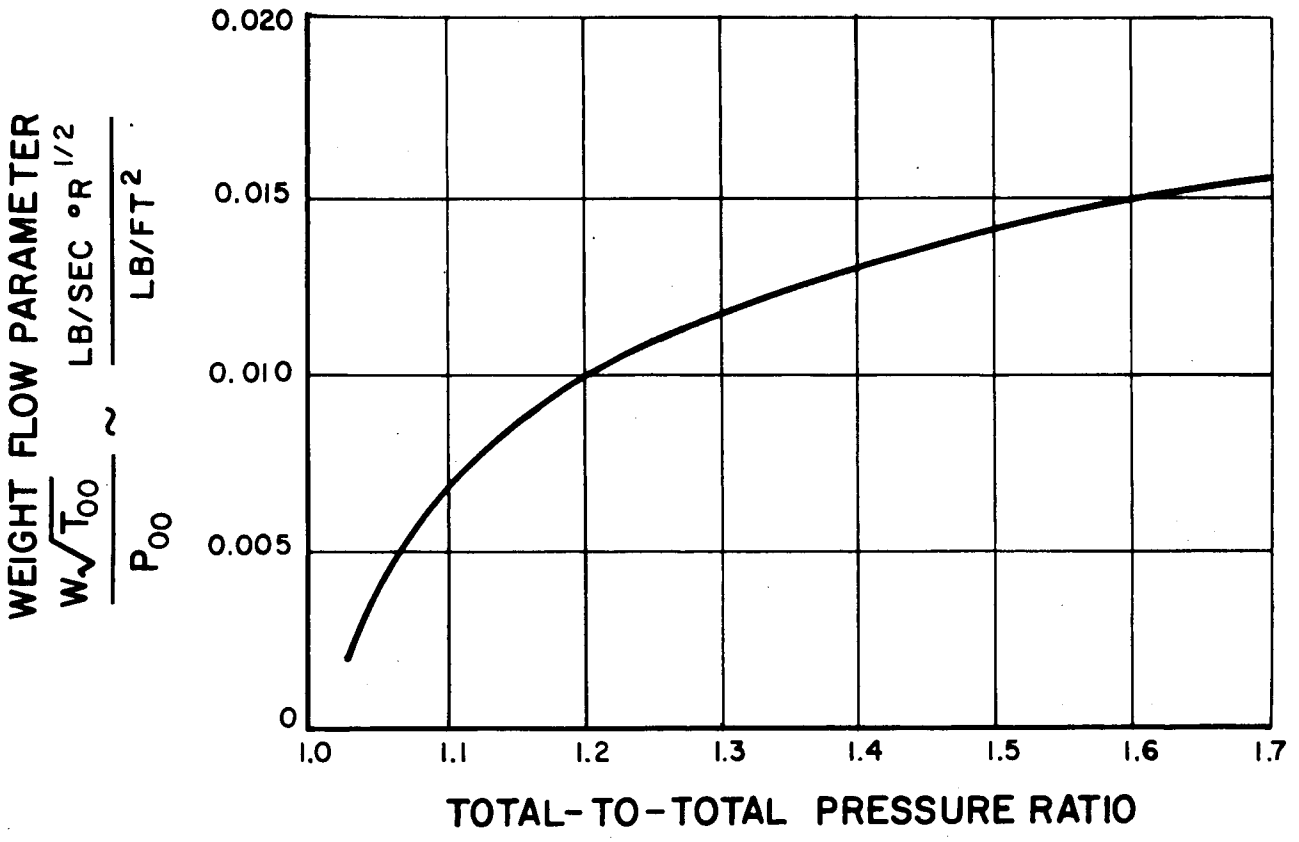

Figure 21 Predicted Weight Flow Parameter

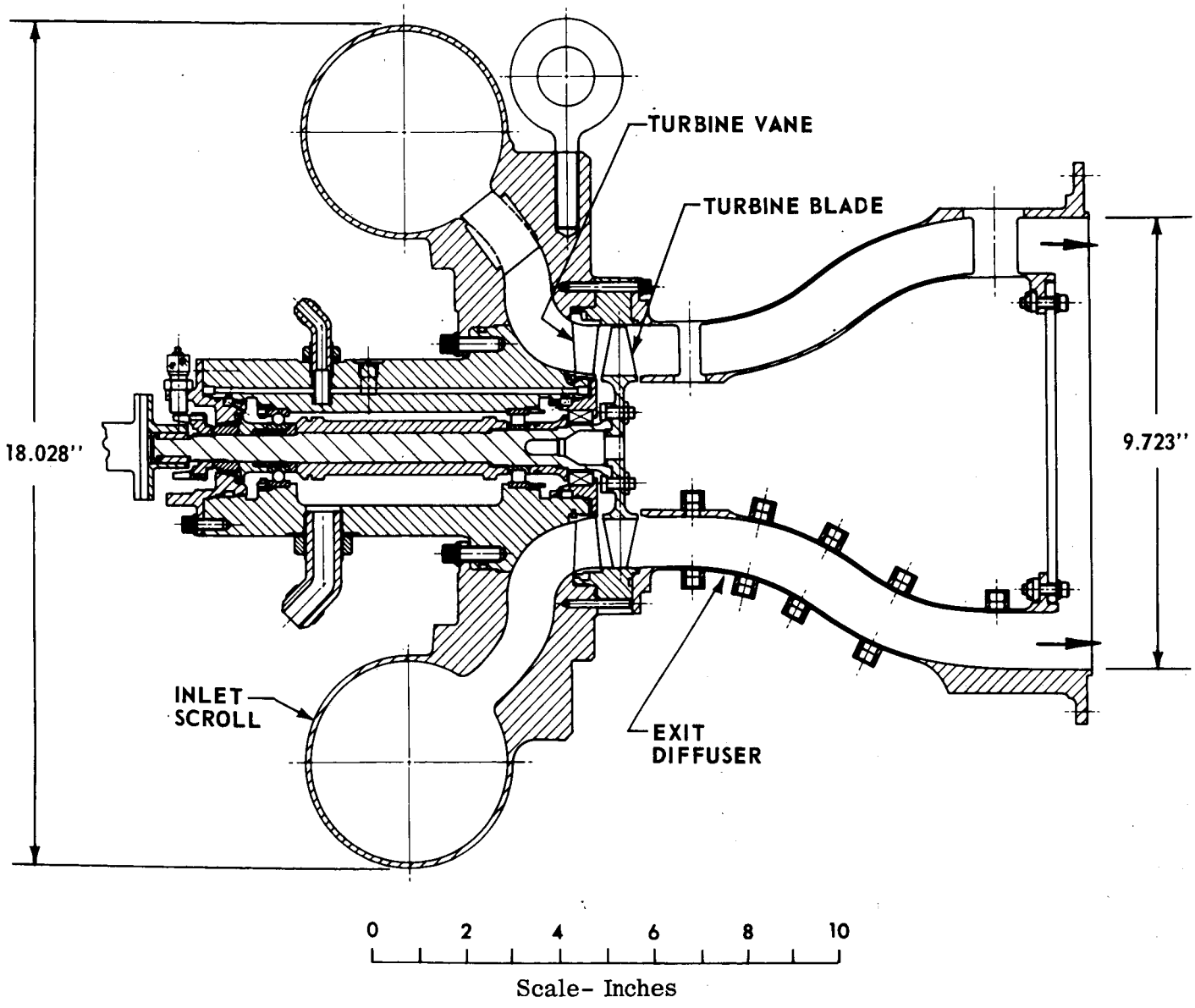

Figure 22 Turbine Research Package M-32725

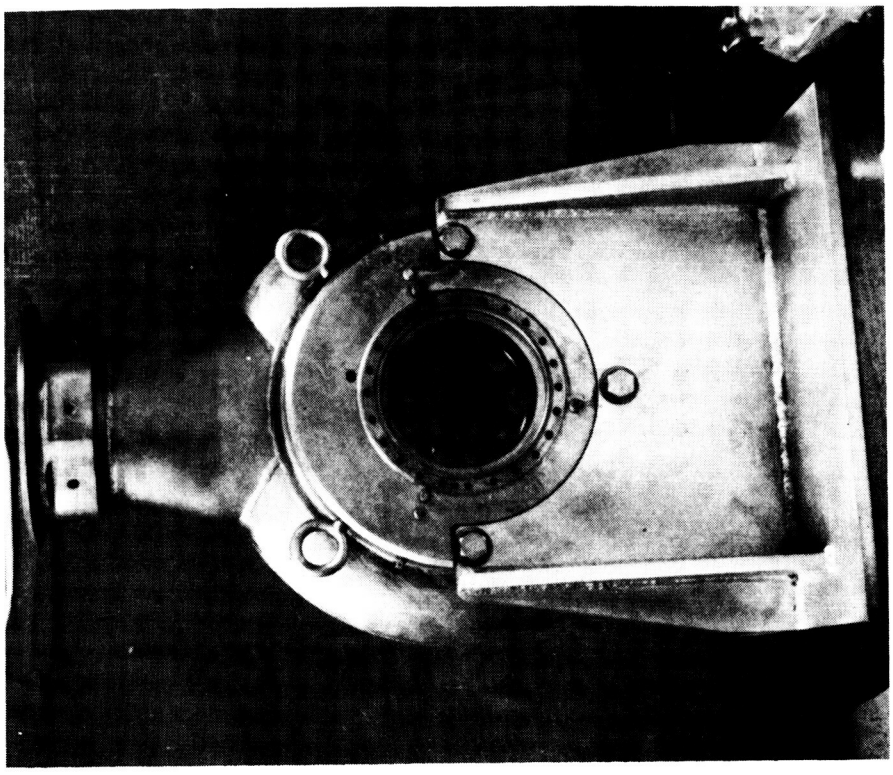

Turbine End

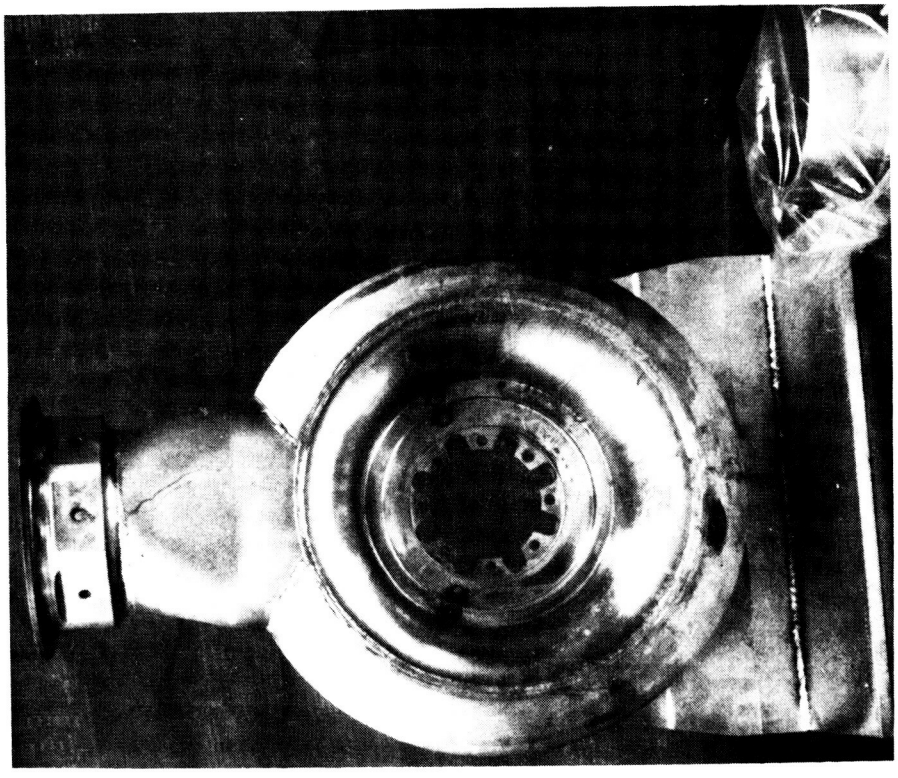

Drive End

Figure 23 Gas Inlet Scroll M-36217

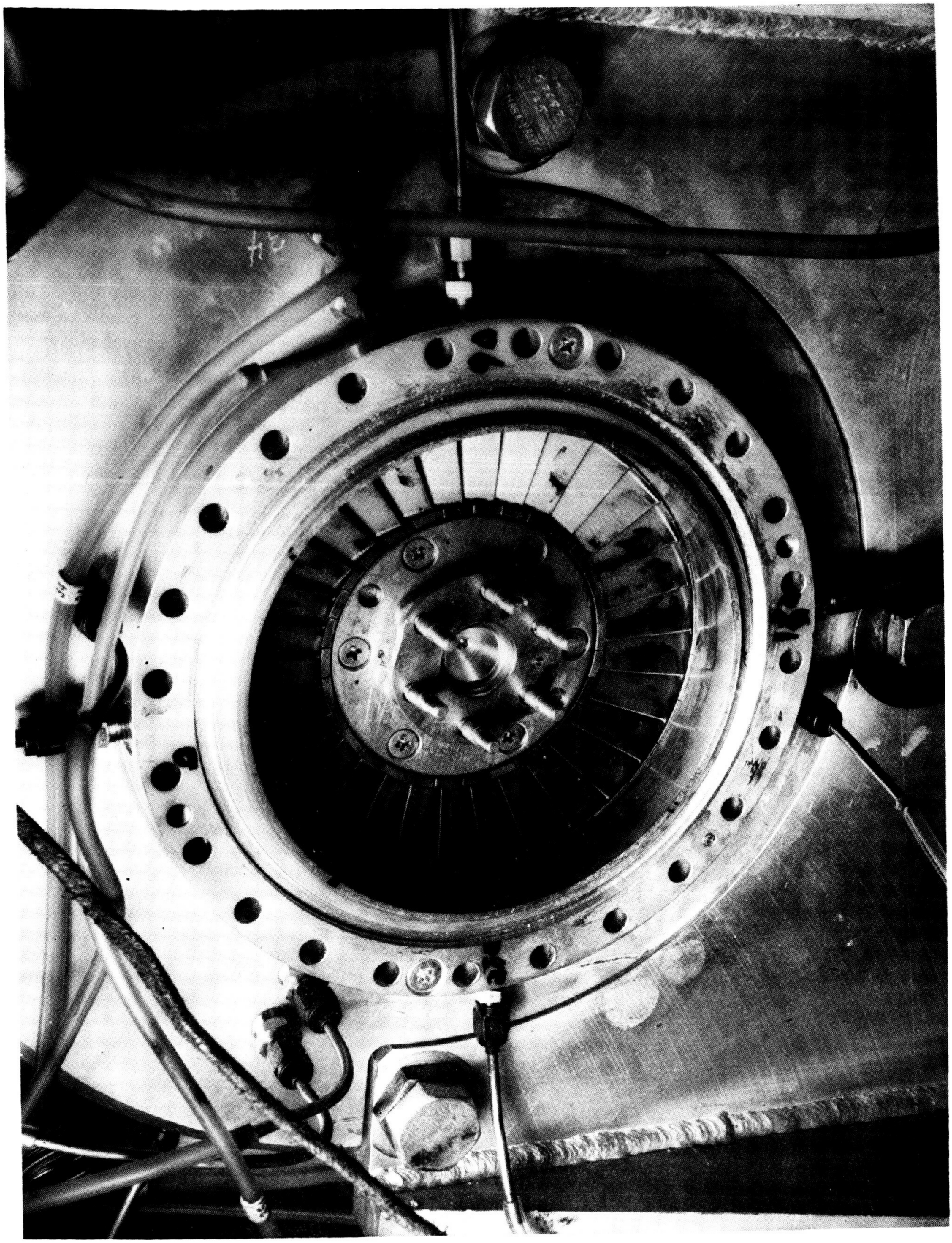

Figure 24 Trailing Edge View of Nozzle X-20154

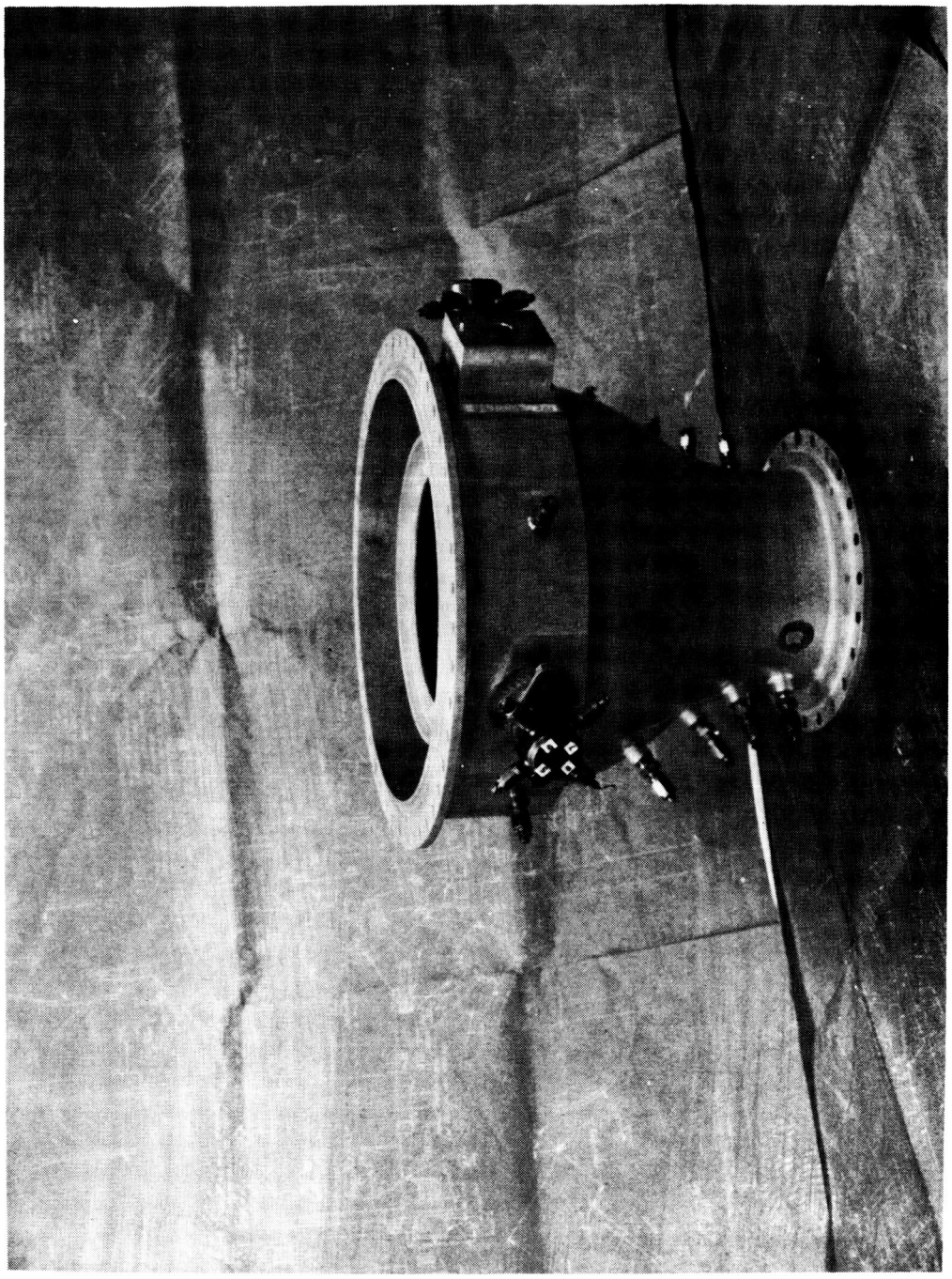

Figure 25 Exit Diffuser

XP-56162

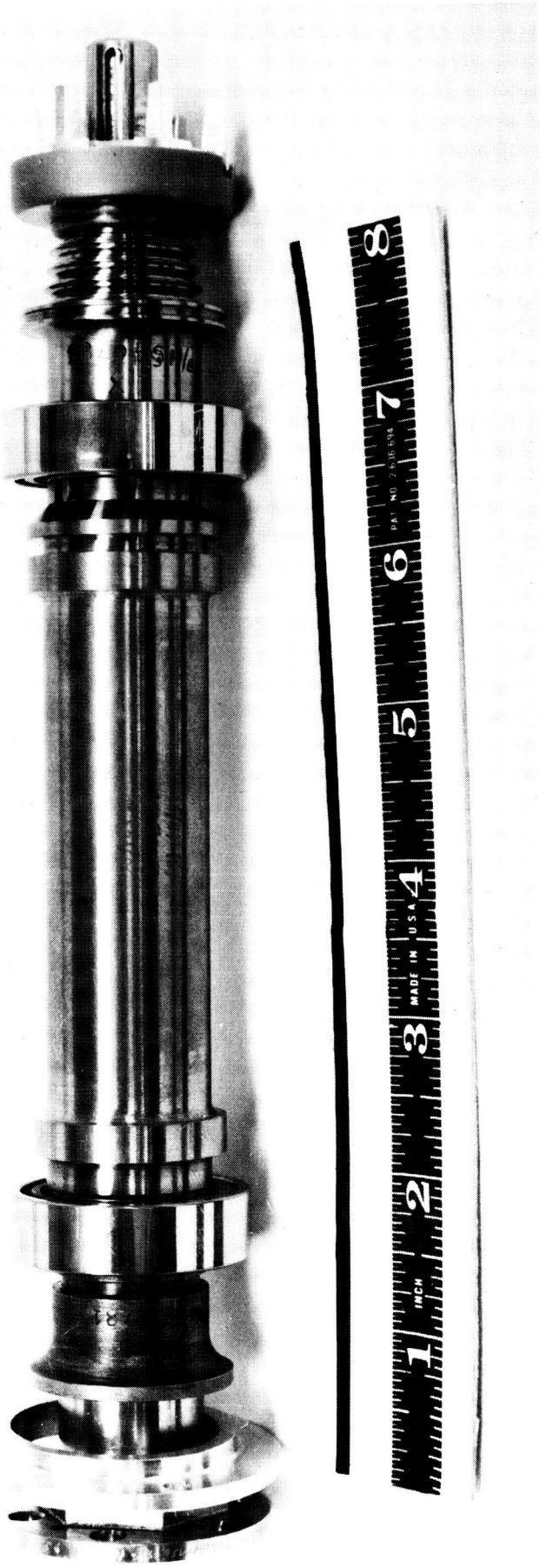

Figure 26 Shaft Assembly X-20687

Figure 27 Labyrinth Seal Housing X-20690

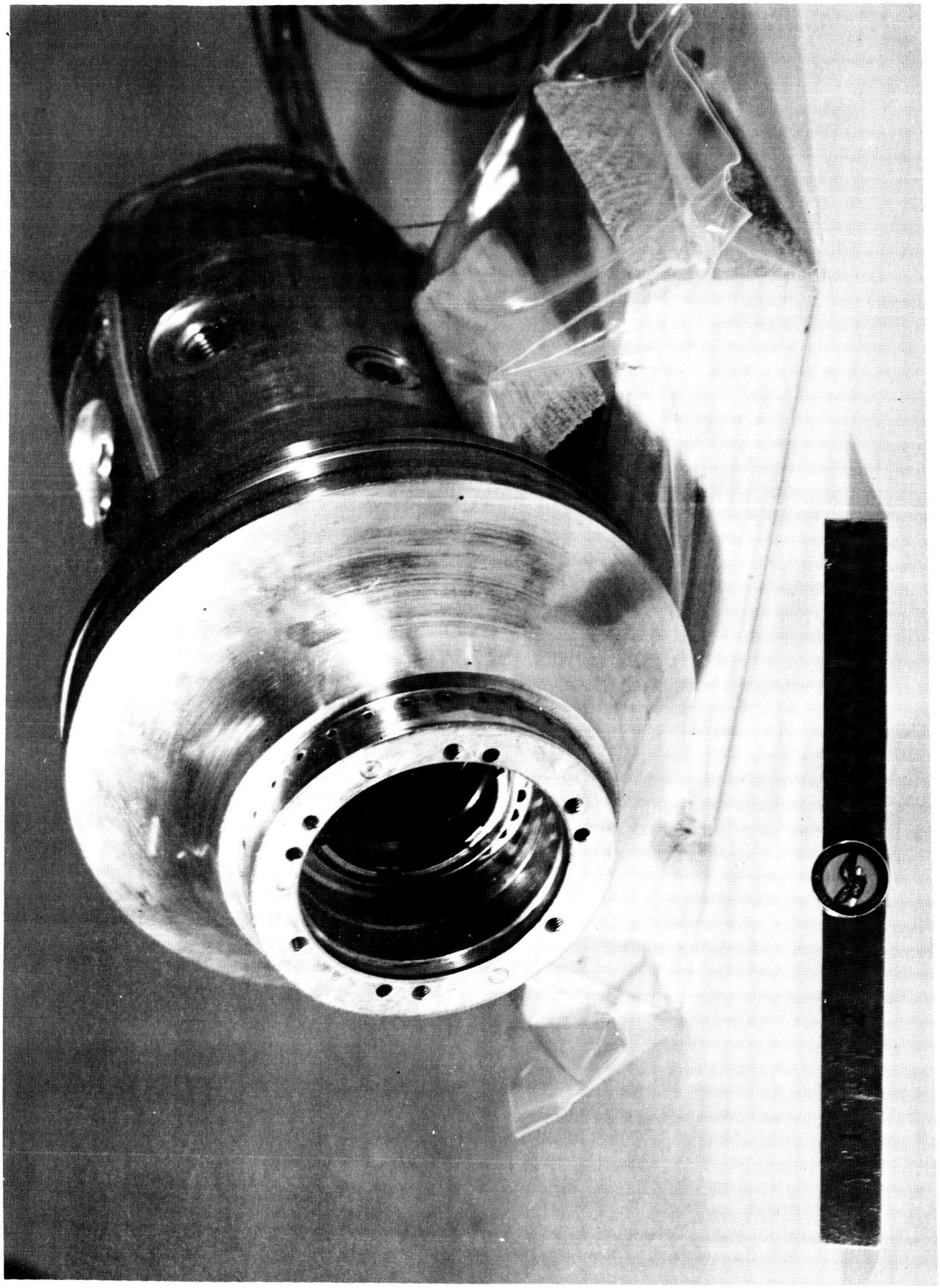

Figure 28 Turbine End of Main Bearing Housing XP-57015

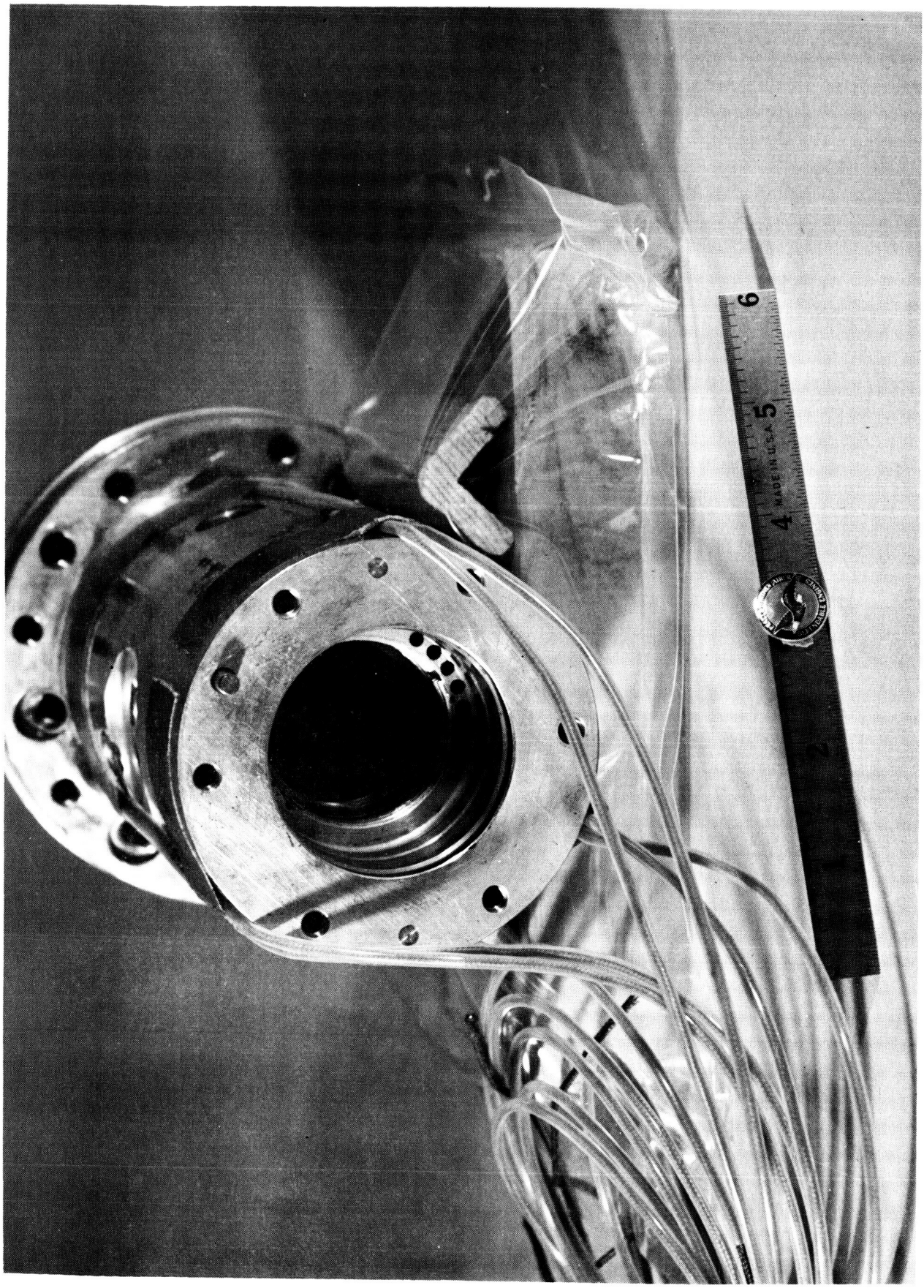

Figure 29 Drive End of Main Bearing Housing XP-57014

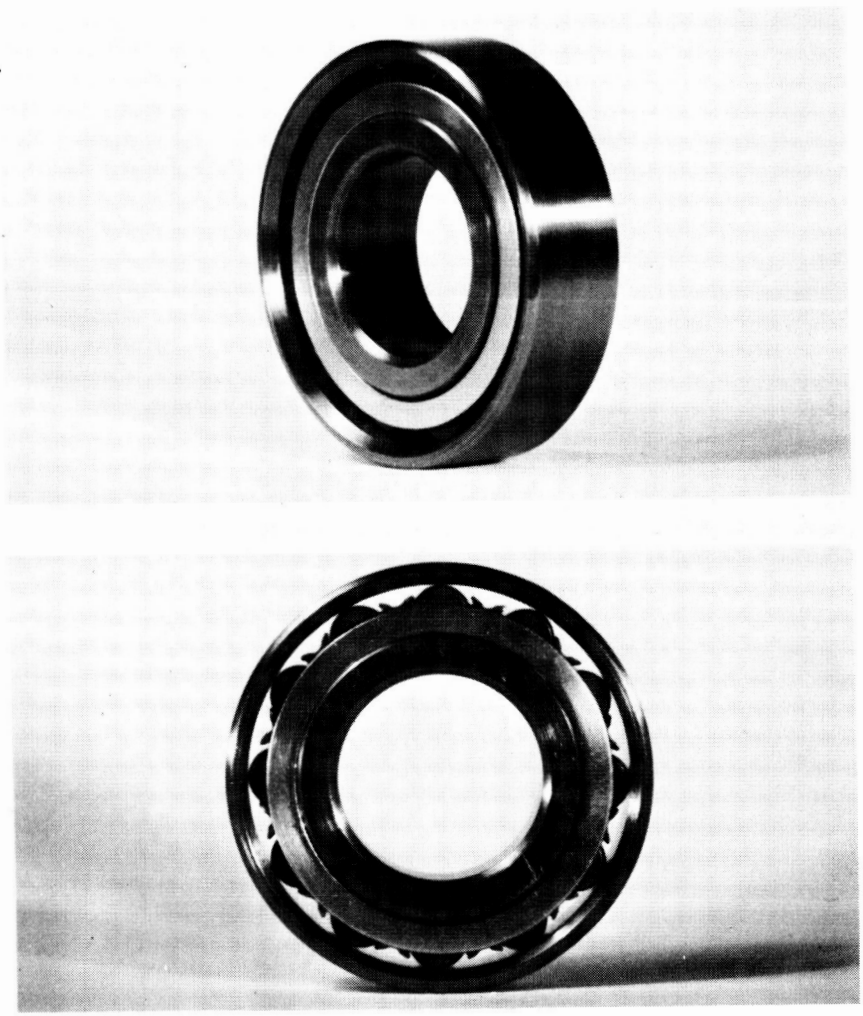

Figure 30 Roller Bearing

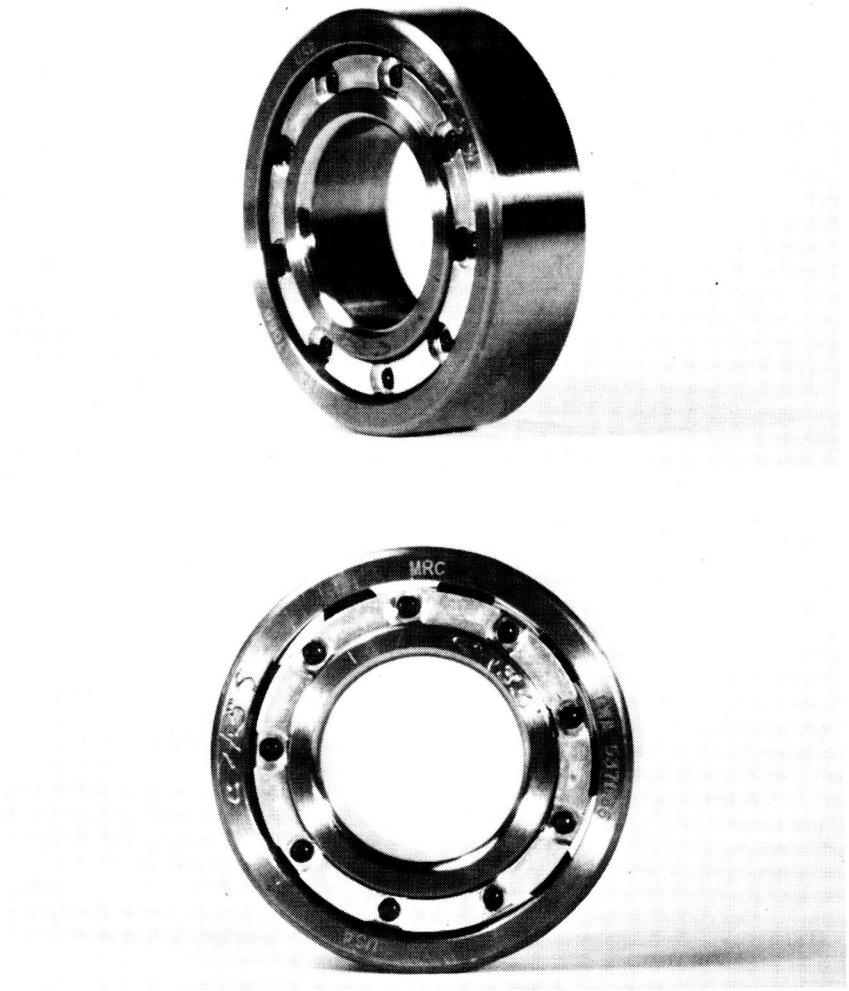

Figure 31 Ball Bearing

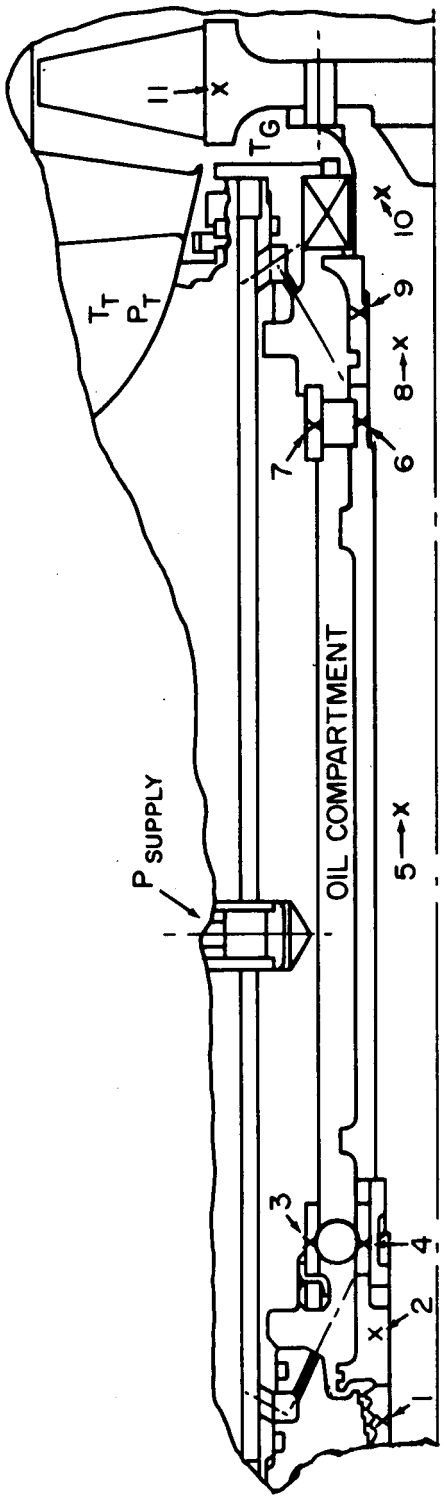

TURBINE CONDITIONS

FLUID - ARGON
T_T = 200 °F
P_T = 13.2 PSIA
N = 30,000 RPM

METAL TEMPERATURES, °F

1	91	7	203
2	97	8	250
3	116	9	260
4	121	10	155
5	100	11	135
6	200		

Figure 32 Thermal Map of Turbine Research Package

Figure 33 Carbon Seal X-19988

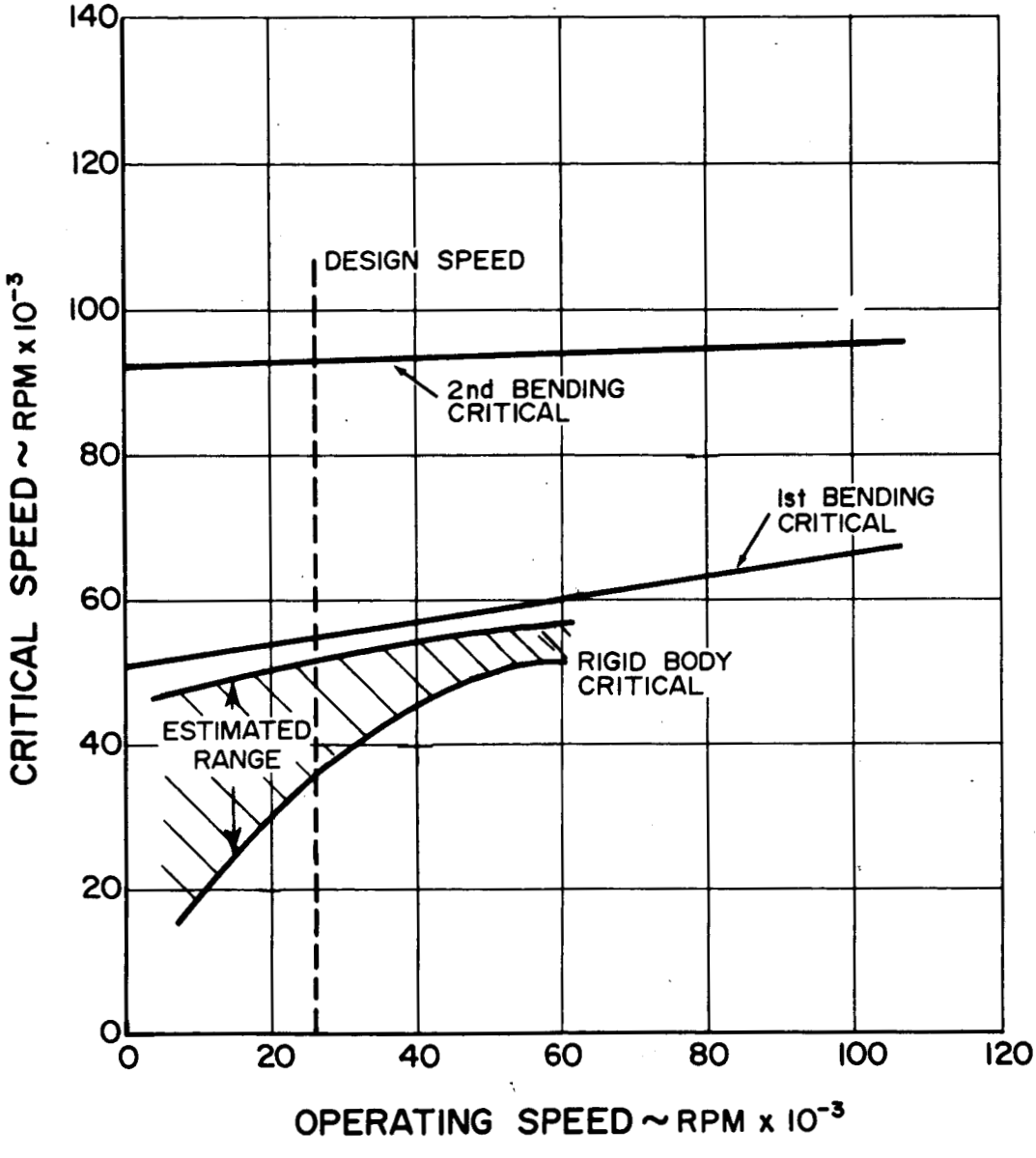

Figure 34 Rotor Critical Speeds

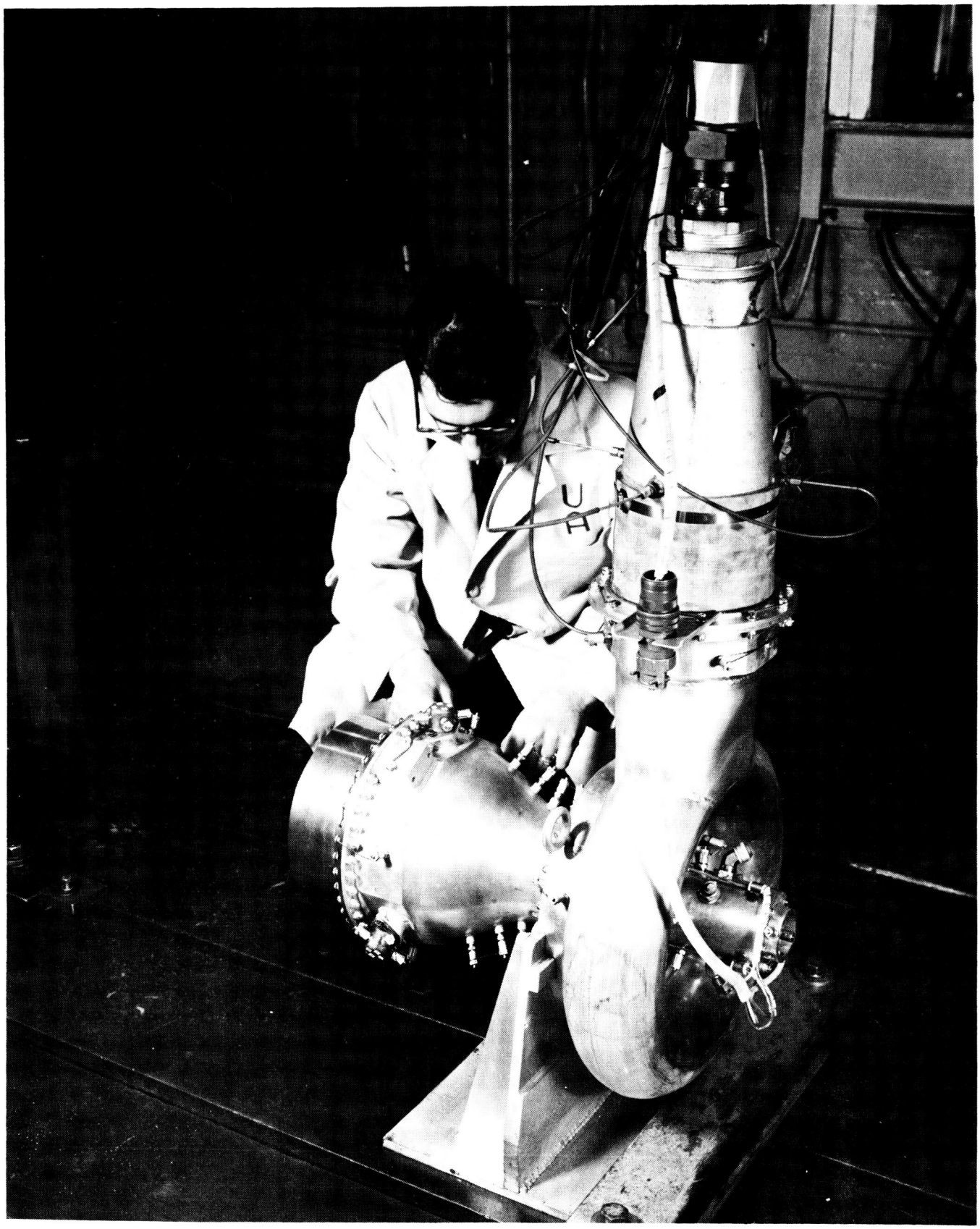

Figure 35 Turbine Research Package Mounted for Acceptance Test XP-62532

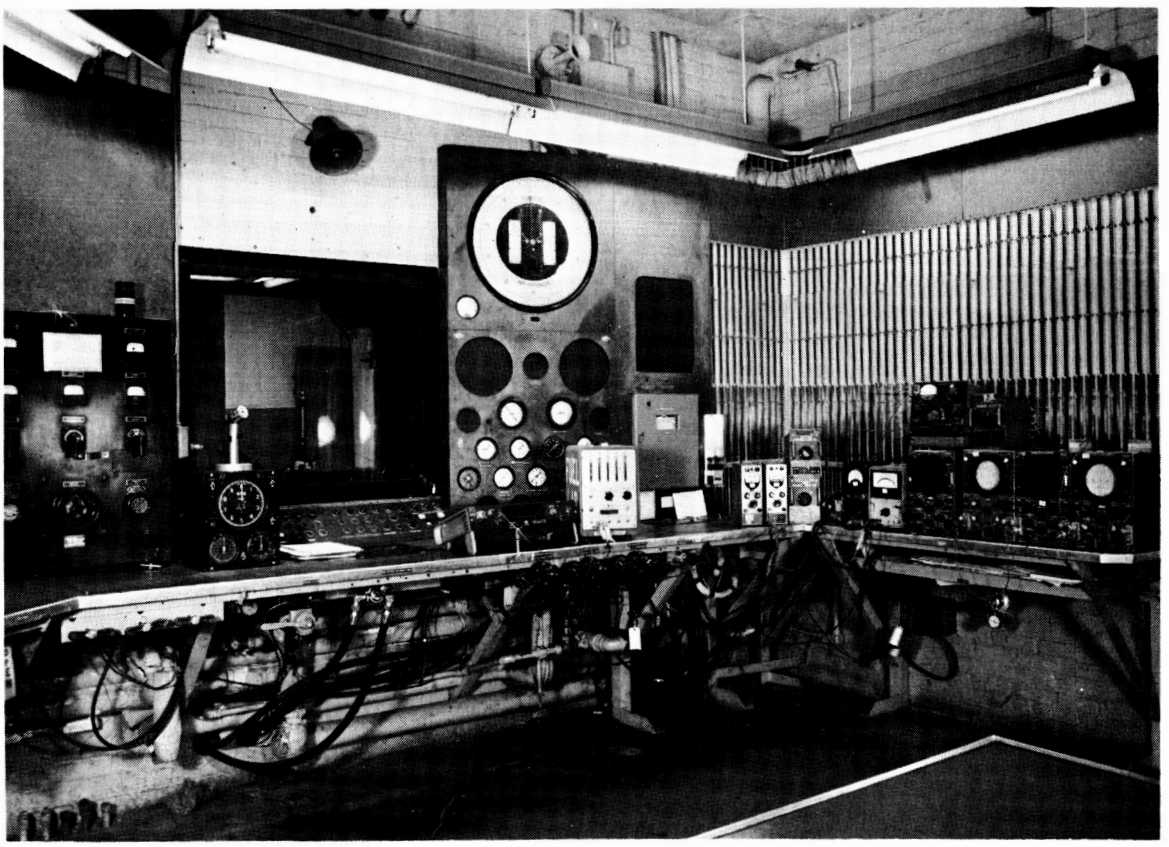

Figure 36 Control Room Used for Test XP-59854

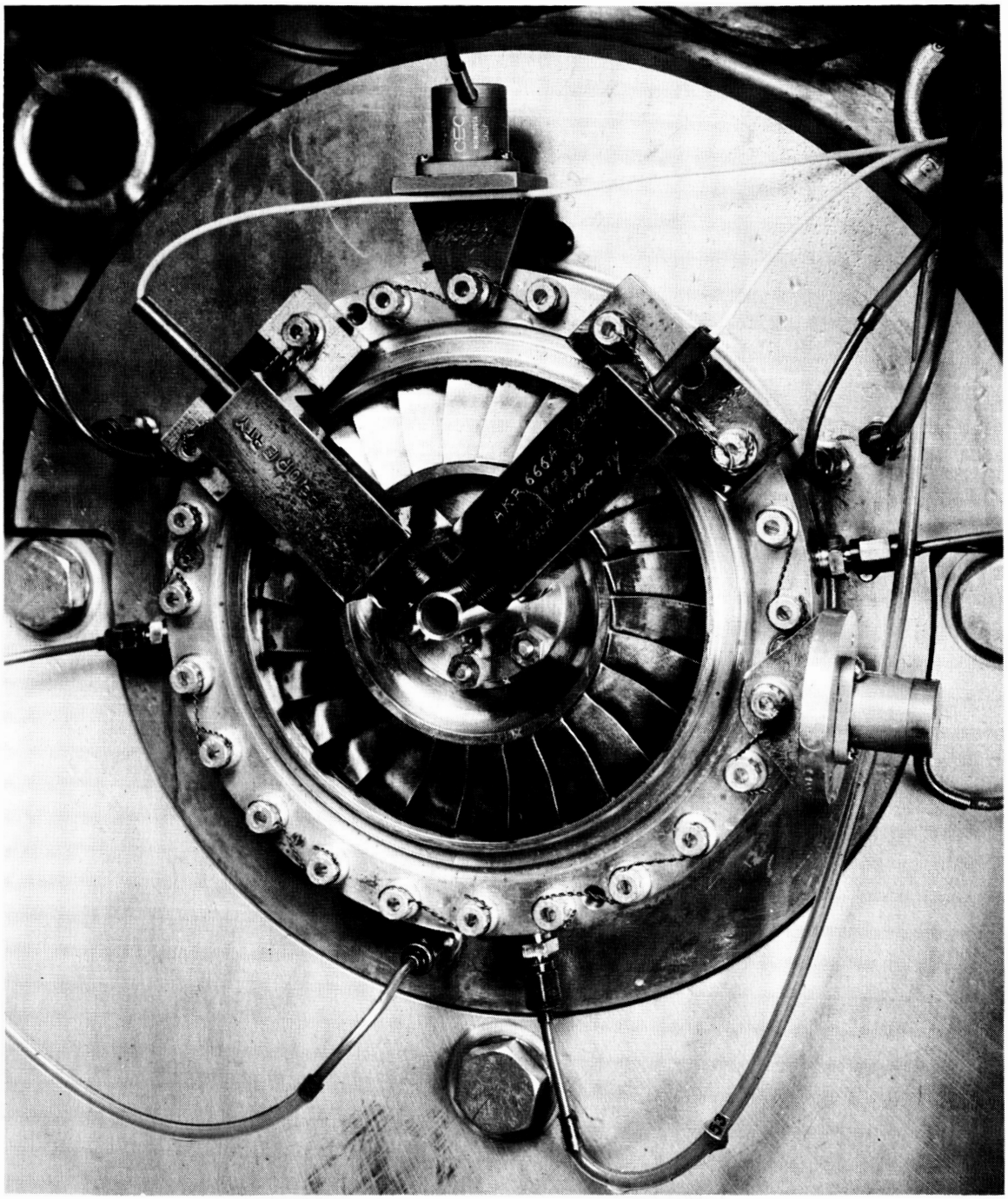

Figure 37 Installation of Proximity Probes at Turbine Disk XP-59862

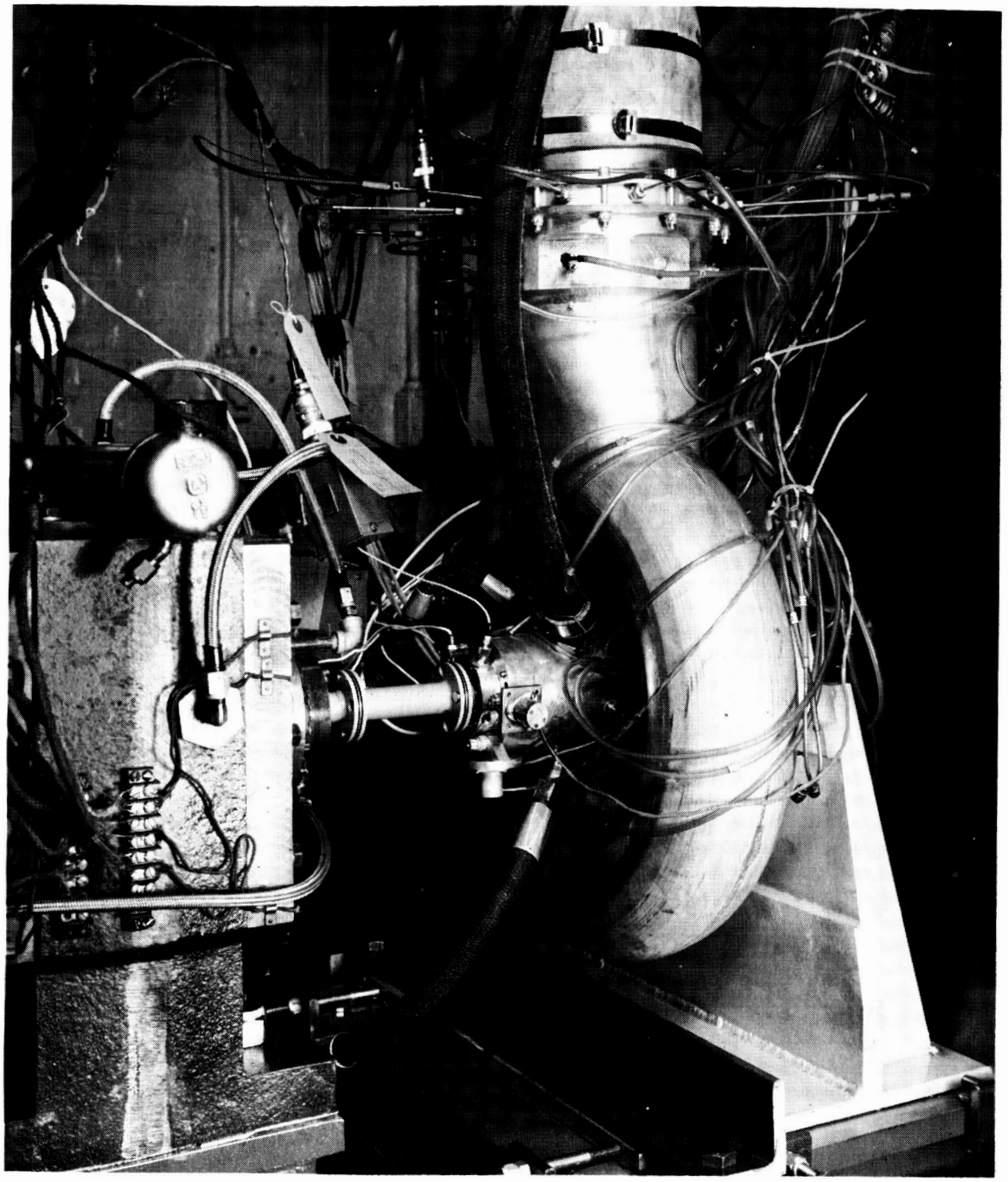

Figure 38 Installation of Proximity Probes at Coupling XP-59859

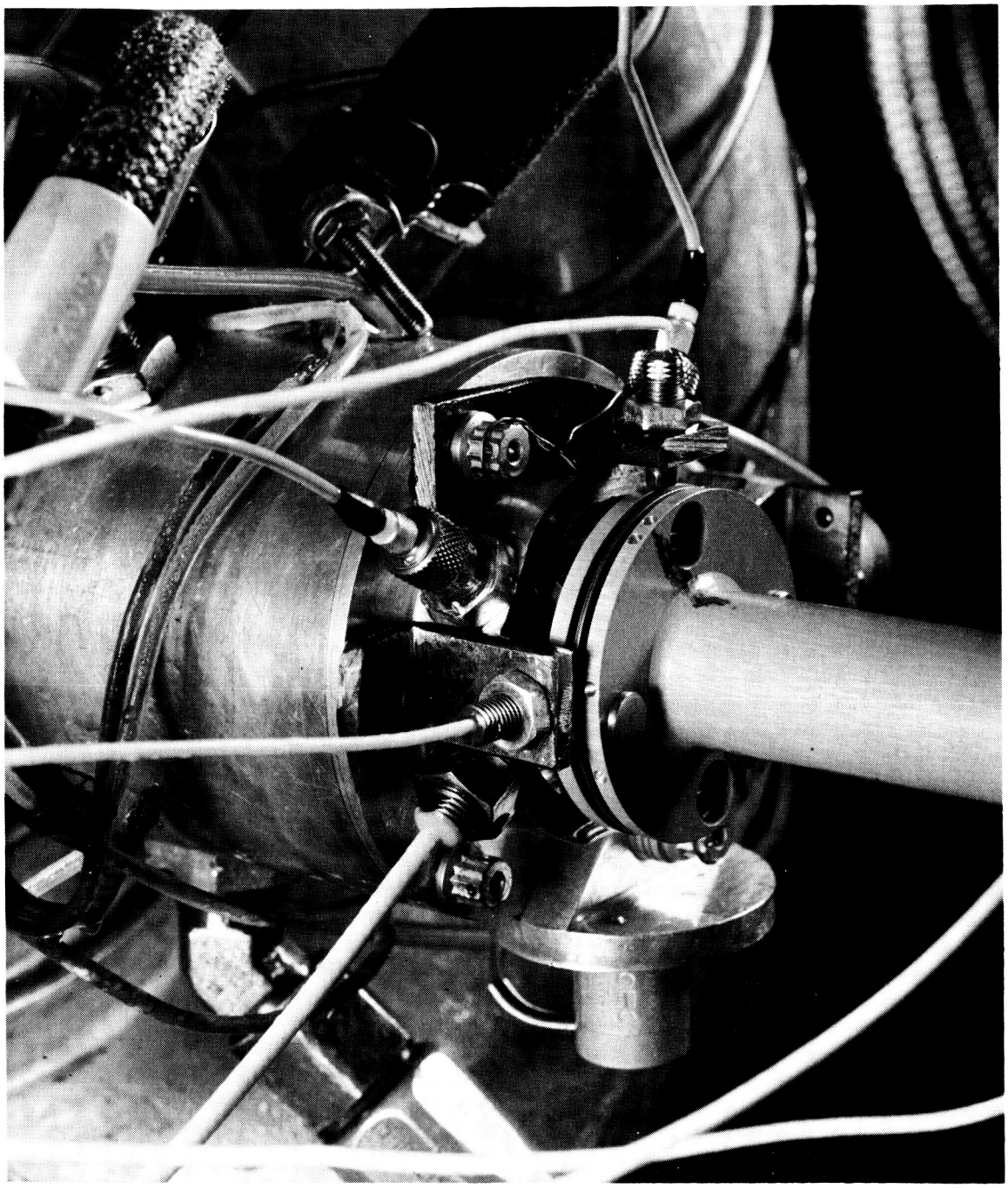

Figure 39 Installation of Proximity Probes at Turbine End of Coupling

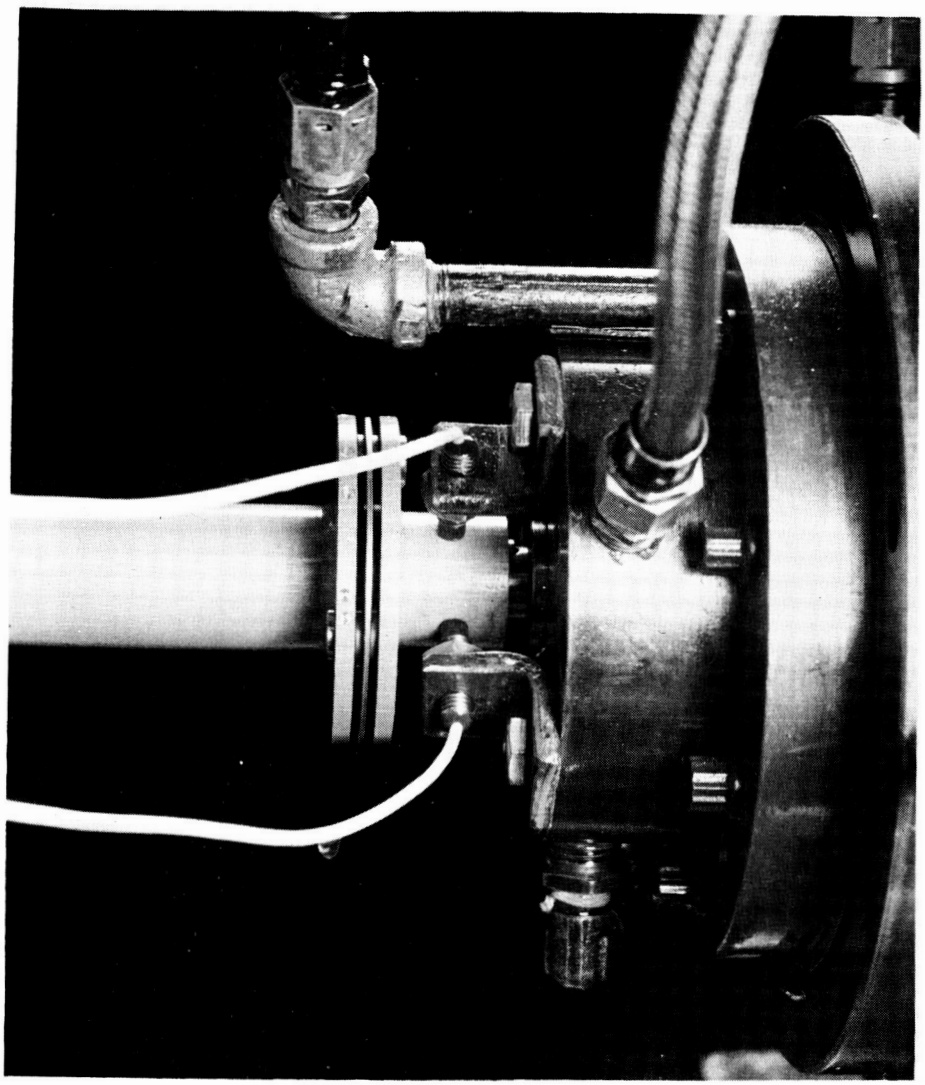

Figure 40 Installation of Proximity Probes at Gearbox End of Coupling

XP-59856

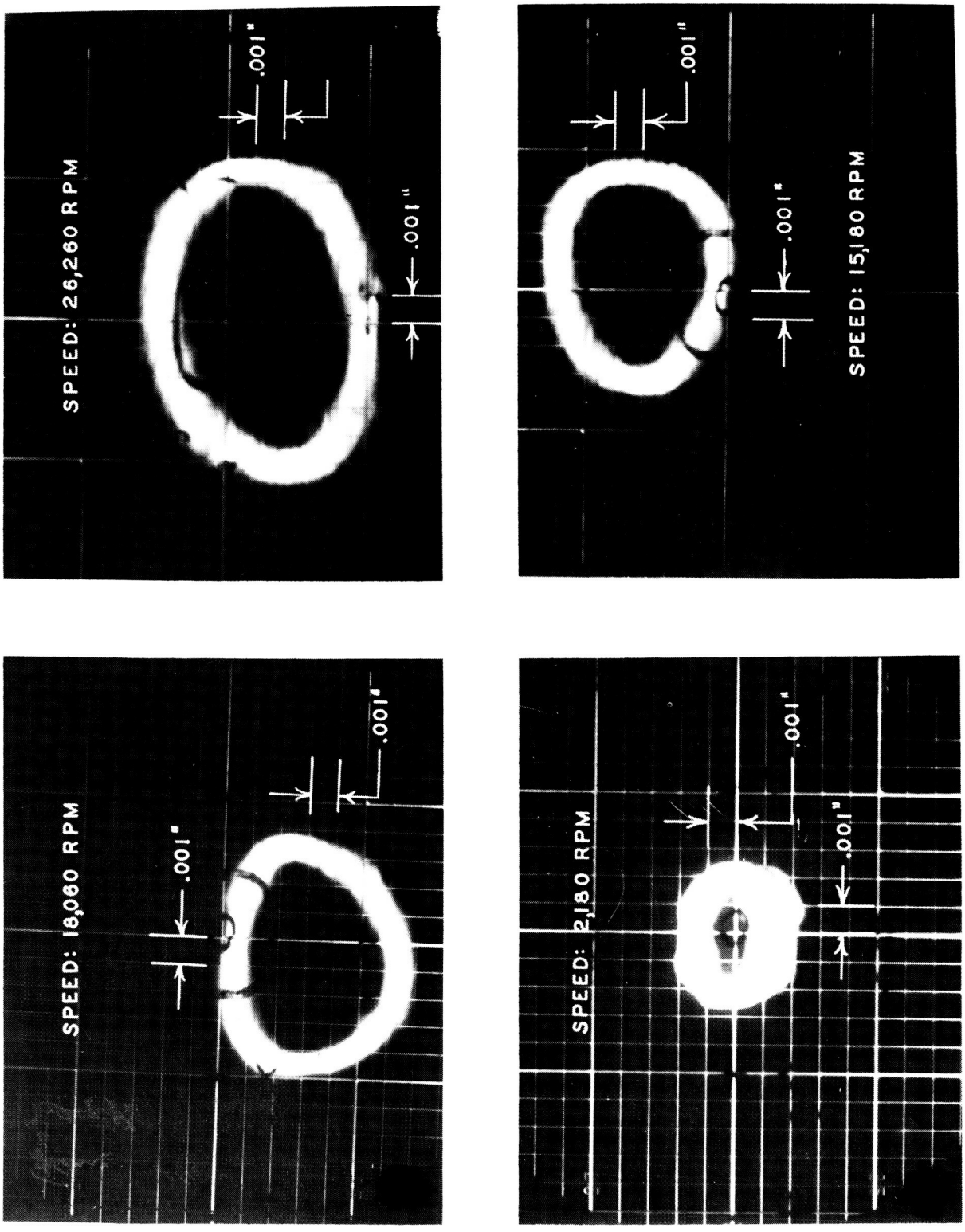

Figure 41 Orbit of Disk End of Turbine Shaft, Coupling Mounted XP-60594

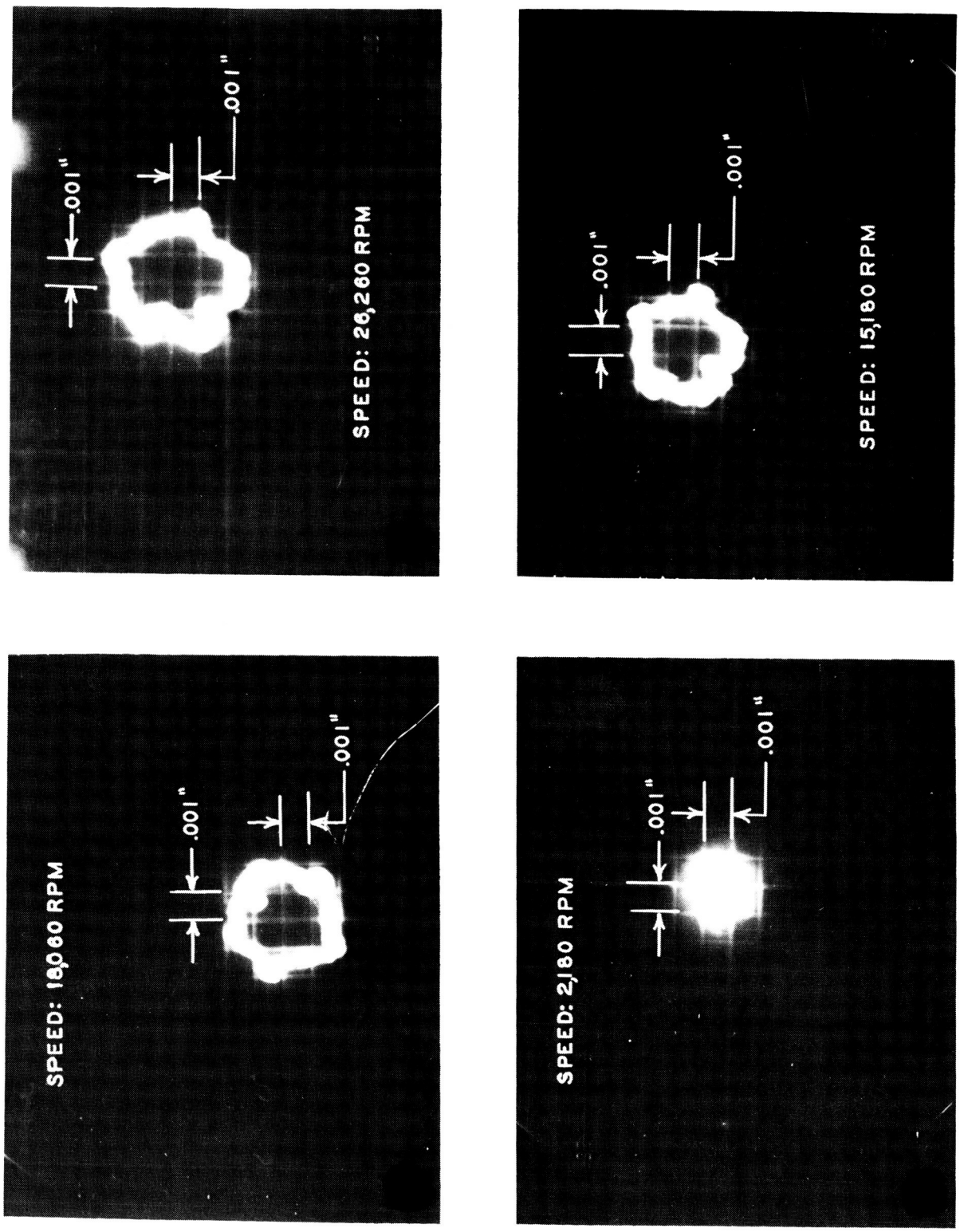

Figure 42 Orbit of Turbine End of Coupling XP-60592

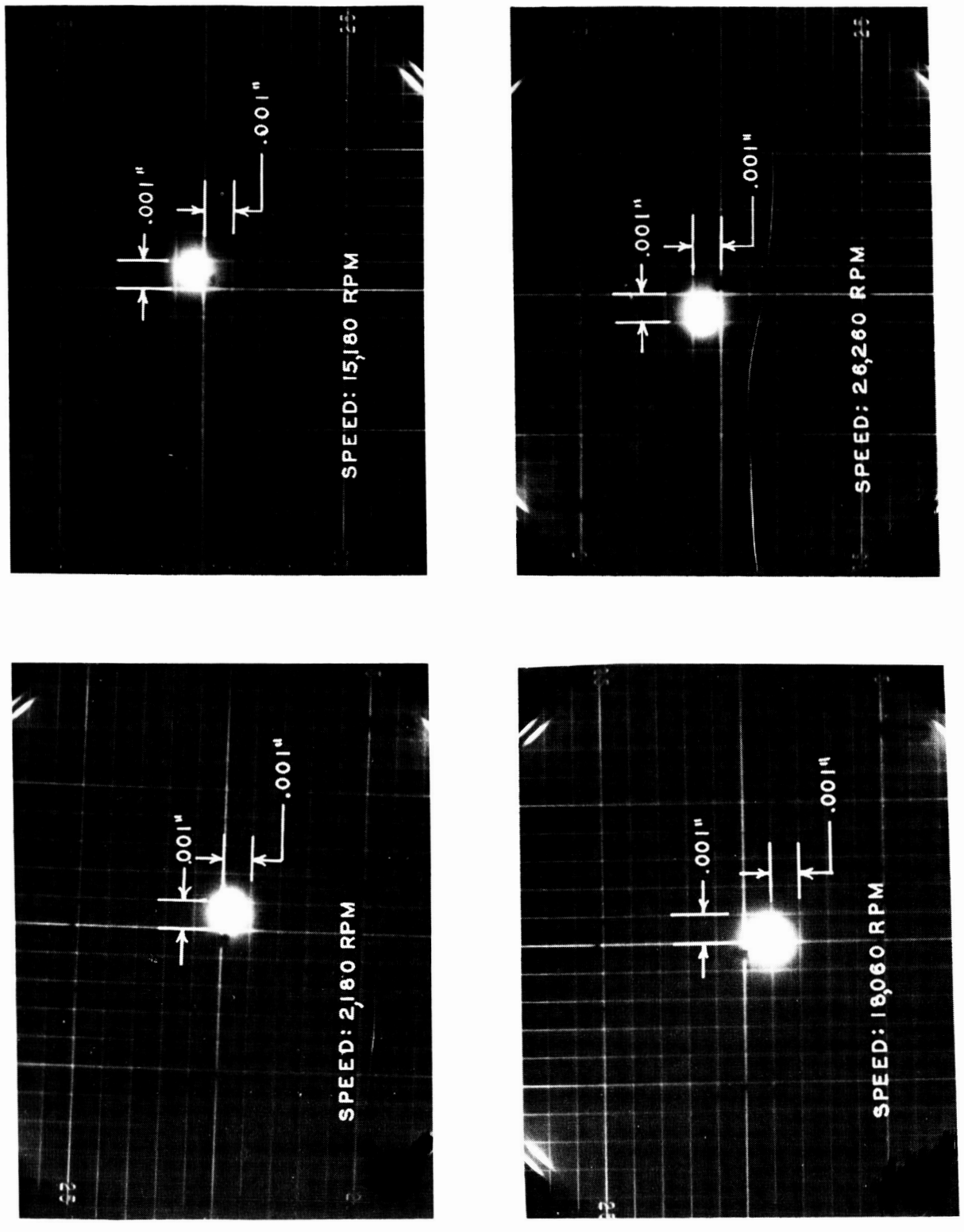

Figure 43 Orbit of Gearbox End of Coupling XP-60595

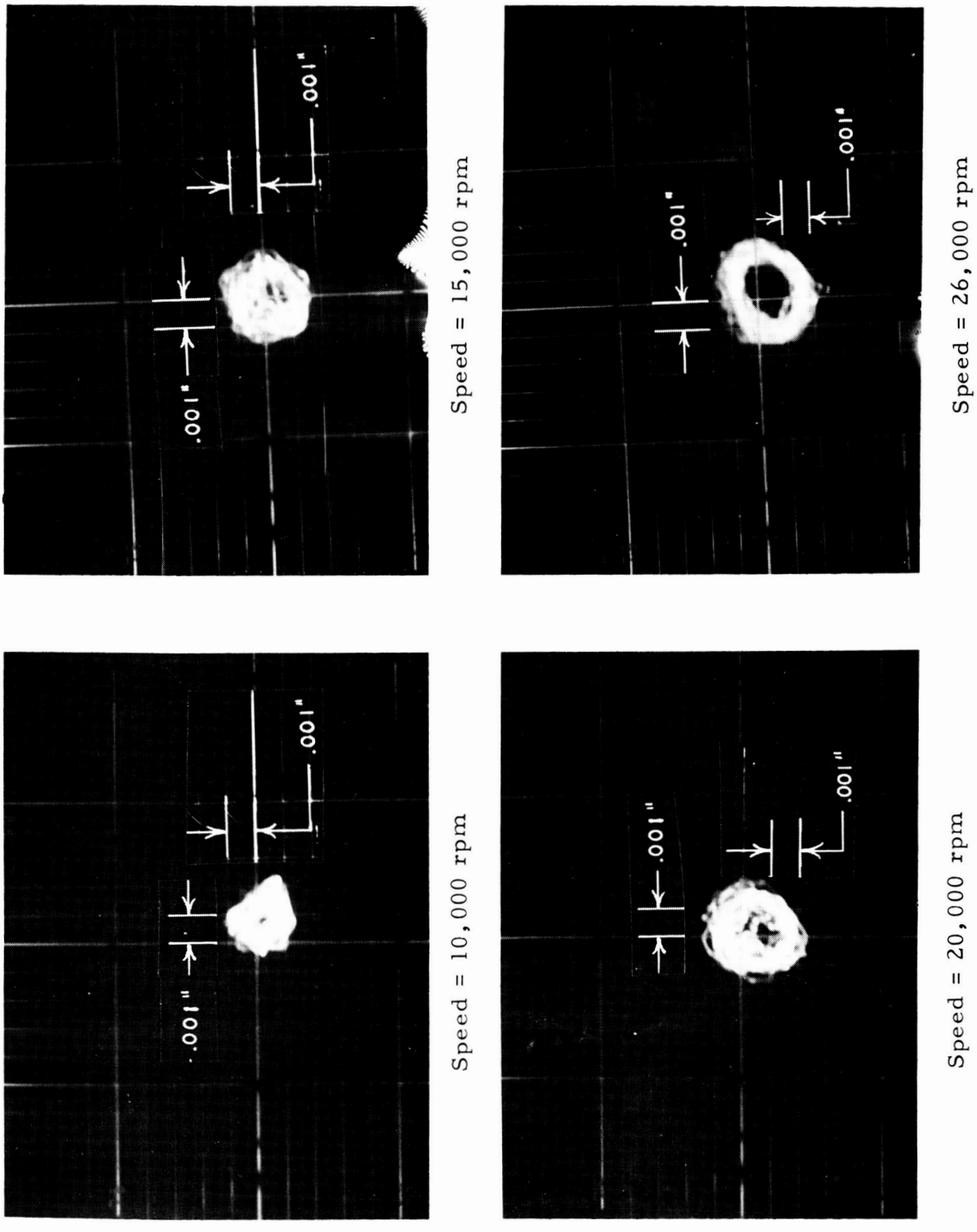

Figure 44 Orbit of Disk End of Turbine Shaft

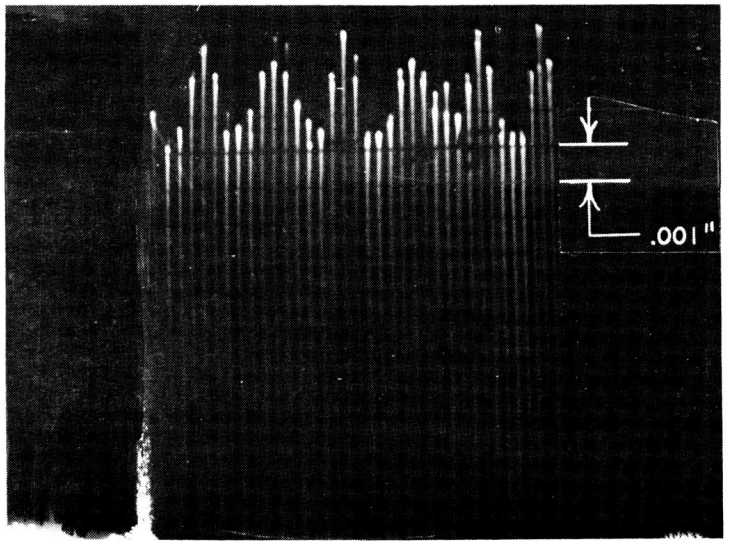

Speed = 10,000 rpm

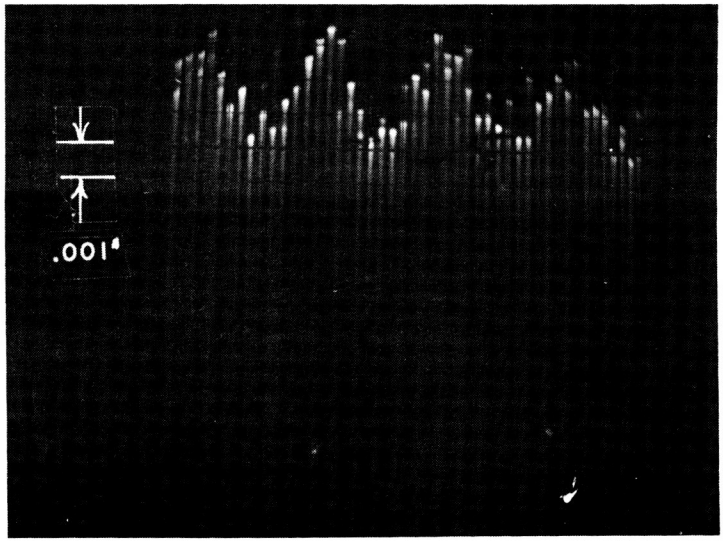

Speed = 15,000 rpm

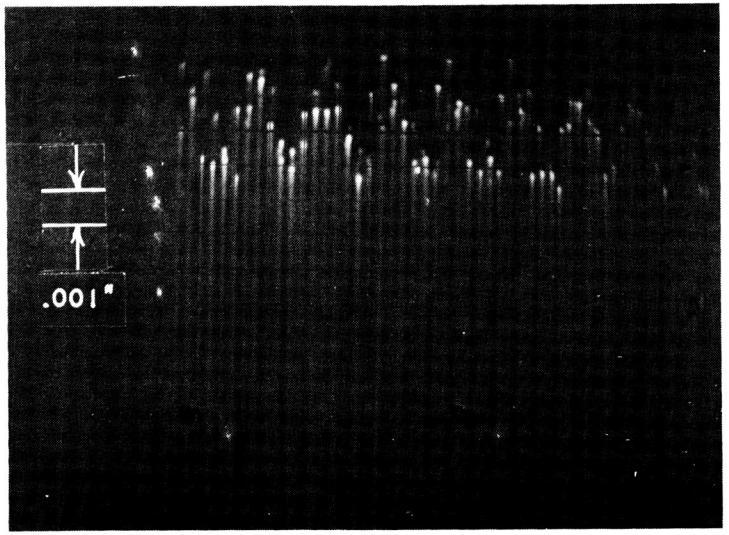

Speed = 20,000 rpm

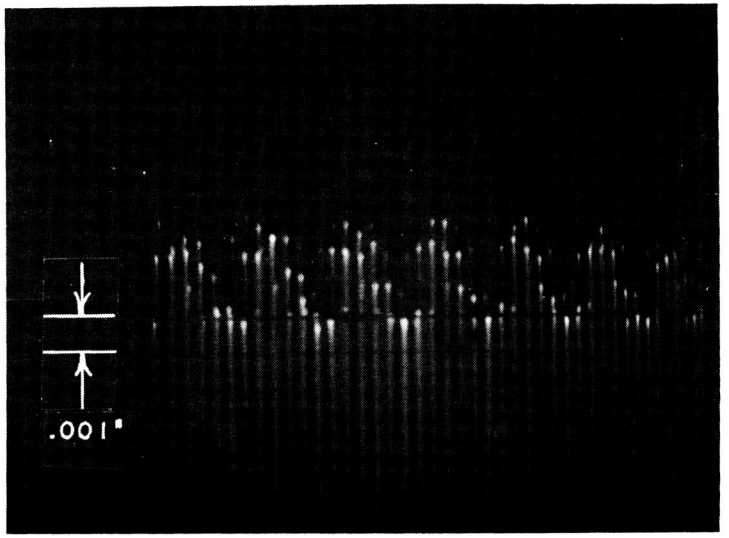

Speed = 26,000 rpm

Figure 45 Radial Deflection Trace of Six-Tooth Speed Gear

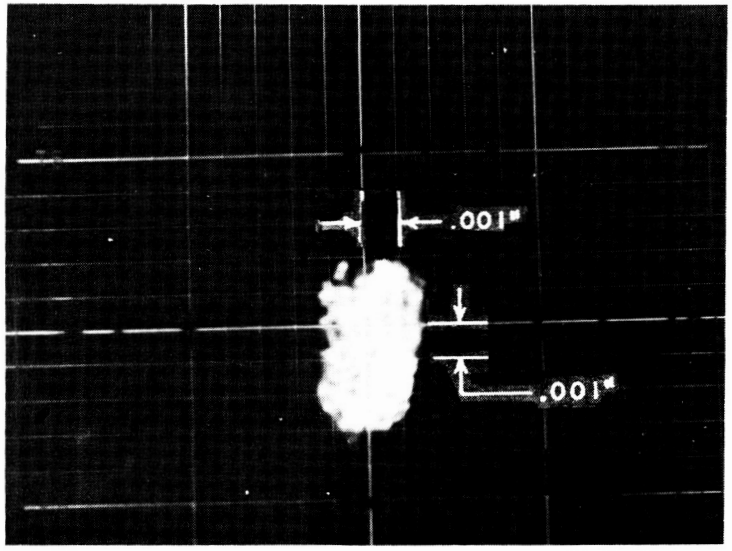

Orbit of Disk End of Turbine Shaft

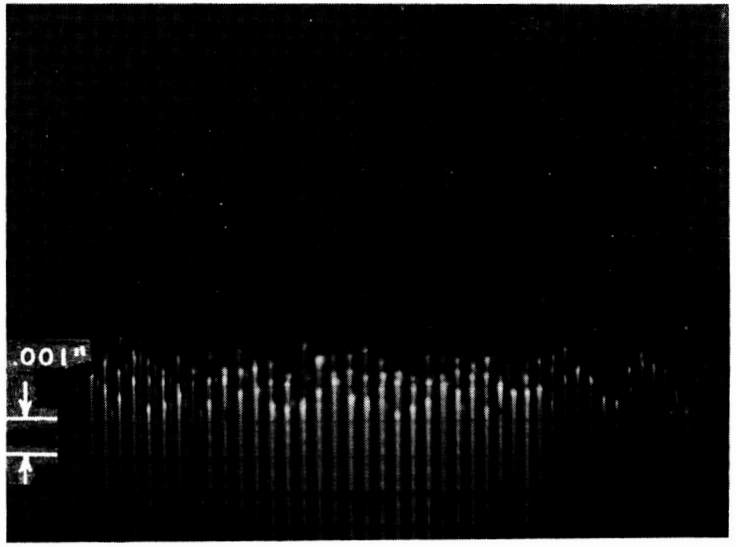

Radial Deflection Trace of Six-Tooth Speed Gear

Figure 46 Test Data at 31,000 rpm

Appendix 1

Measured Turbine Research Package Clearances

	Clearance-inch
radial tip clearance of rotor	0.010 to 0.0125
axial clearance between nozzle and rotor at hub diameter	0.070
axial clearance between rotor and case at hub diameter	0.102
total shaft axial play	0.0085
total shaft radial play at disc end	0.0025
carbon face seal compression	0.075
labyrinth seal radial clearance	0.010

FINAL REPORT
TURBINE RESEARCH PACKAGE FOR RESEARCH AND DEVELOPMENT OF HIGH PERFORMANCE AXIAL FLOW TURBINE-COMPRESSOR

Written by

R. Cohen, W. K. Gilroy, E. D. Havens

Approved by

P. Bolan

ABSTRACT

The National Aeronautics and Space Administration is conducting an evaluation of candidate Brayton-cycle turbomachinery configurations. As a part of this program, Pratt & Whitney Aircraft has designed a turbine-compressor incorporating a single-stage axial-flow turbine driving a six-stage axial-flow compressor supported on gas bearings. A turbine research package was provided to permit evaluation of aerodynamic performance of the turbine using low temperature gas. The turbine research package incorporates oil-lubricated rolling-contact bearings. The aerodynamic and mechanical design of the turbine research package is discussed and the results of mechanical testing are presented.

Distribution List
Contract NAS3-4179

National Aeronautics and Space Administration
Washington, D. C. 20546
Attention: Dr. Fred Schulman, RNP — 1
Herbert D. Rochen, RNP — 1
S. V. Manson, RNP — 1
Arvin Smith, RNW — 1

National Aeronautics and Space Administration
Lewis Research Center
21000 Brookpark Road
Cleveland, Ohio 44135
Attention: Jack A. Heller, MS 500-201 — 3
J. E. Dilley, MS 500-309 — 1
J. J. Weber, MS 3-19 — 1
Dr. B. Lubarsky, MS 500-201 — 1
D. G. Beremand, MS 500-201 — 1
J. H. Dunn, MS 500-201 — 1
J. P. Joyce, MS 500-201 — 1
H. B. Tryon, MS 500-201 — 1
I. I. Pinkel, MS 5-3 — 1
W. L. Stewart, MS 77-2 — 1
H. E. Rohlik, MS 77-2 — 1
C. L. Ball, MS 5-9 — 1
M. G. Kofskey, MS 77-2 — 1
D. C. Guentert, MS 500-201 — 1
D. T. Bernatowicz, MS 500-201 — 1
T. A. Moss, MS 500-201 — 1
V. F. Hlavin, MS 3-14 — 1
D. E. Holeski, MS 77-2 — 1
F. J. Dutee, MS 21-4 — 1
R. Y. Wong, MS 77-2 — 1
Report Control Office, MS 5-5 — 1
Reliability & Quality Assurance Office, MS 500-203 — 1
Library, MS 60-3 — 2

NASA Ames Research Center
Moffett Field, California 94035 — 1
Attention: Library

NASA Flight Research Center
P. O. Box 273, Edwards, California 93523
Attention: Library — 1

NASA Goddard Space Flight Center
Greenbelt, Maryland 20771
Attention: Library — 1

NASA Langley Research Center
Langley Station, Hampton, Virginia 23365
Attention: Library — 1

NASA Manned Spacecraft Center
Houston, Texas 77058
Attention: Anthony Redding, — 1
Library, — 1

NASA Marshall Space Flight Center
Huntsville, Alabama 35812
Attention: Library — 1

NASA Western Operations Office
150 Pico Boulevard
Santa Monica, California 90406
Attention: Library — 1

NASA Jet Propulsion Laboratory
4800 Oak Grove Drive
Pasadena, California 91103
Attention: Library — 1

National Aeronautics and Space Administration
Scientific & Technical Information Facility
P.O. Box 33, College Park, Maryland 20740
Attention: Acquisitions Branch, SQT-34054 — 1 + 1 repro

NASA Lewis Research Center Resident Office
Pratt & Whitney Aircraft
West Palm Beach, Florida 33402
Attention: George K. Fischer — 1

U.S. Army Engineer R&D Laboratories
Gas Turbine Test Facility
Fort Belvoir, Virginia 22060
Attention: W. Crim — 1

Office of Naval Research
Department of the Navy
Washington, D. C. 20025
Attention: Dr. Ralph Roberts — 1

Bureau of Naval Weapons
Department of the Navy
Washington, D. C. 20025
Attention: Code RAPP — 1

Bureau of Ships
Department of the Navy
Washington, D. C. 20025
Attention: G. L. Graves — 1

Air Force Systems Command
Aeronautical Systems Division
Wright-Patterson Air Force Base, Ohio 45433
Attention: Library — 1

Wright-Patterson Air Force Base, Ohio 45433
Attention: Robin Chasman, APFL — 1
George Thompson, APFL — 1

Institute for Defense Analyses
400 Army - Navy Drive
Arlington, Virginia 22202
Attention: Library — 1

University of Pennsylvania
Power Information Center
Moore School Building
200 South 33rd Street
Philadelphia, Pennsylvania 19104 — 1

Massachusetts Institute of Technology
Cambridge, Massachusetts 02139
Attention: Library — 1

University of Virginia
Department of Mechanical Engineering
Charlottesville, Virginia 22903
Attention: Dr. J. E. Gunter, Jr. — 1

Aerojet General Corporation
Azusa, California 91703
Attention: Library — 1

AiResearch Manufacturing Company
The Garrett Corporation
402 South 36th Street
Phoenix, Arizona 85034
Attention: Library — 1

AiResearch Manufacturing Company
The Garrett Corporation
9851 Sepulveda Boulevard
Los Angeles, California 90009
Attention: Library — 1

Bendix Research Laboratories Division
Southfield (Detroit), Michigan 48232
Attention: Library — 1

The Boeing Company
Aero-Space Division
Box 3707, Seattle, Washington 98124
Attention: Library — 1

Borg-Warner Corporation
Pesco Products Division
24700 North Miles Road
Bedford, Ohio 44014
Attention: Library — 1

Consolidated Controls Corporation
15 Durant Avenue
Bethel, Connecticut 06801
Attention: Library — 1

Continental Aviation & Engineering Corporation
12700 Kercheval Avenue
Detroit, Michigan 48215
Attention: Library — 1

Curtiss-Wright Corporation
Wright Aero Division
Main and Passaic Streets
Woodridge, New Jersey 07075
Attention: Library — 1

Douglas Aircraft Company
3000 Ocean Park Boulevard
Santa Monica, California 90406
Attention: Library — 1

Franklin Institute Laboratories
Benjamin Franklin Parkway at 20th St.
Philadelphia, Pennsylvania 19103
Attention: Otto Decker — 1

General Dynamics Corporation
16501 Brookpark Road
Cleveland, Ohio 44142
Attention: Library — 1

General Electric Company
Flight Propulsion Laboratory Division
Cincinnati, Ohio 45215
Attention: Library — 1

General Electric Company
Mechanical Technology Laboratory
Schenectady, New York 12301
Attention: Library — 1

General Electric Company
Missile & Space Vehicle Department
3198 Chestnut Street
Philadelphia, Pennsylvania 19104
Attention: Library — 1

General Motors Corporation
Indianopolis, Indiana 46206
Attention: Library — 1

Lear Siegler, Inc.
3171 S. Bundy Drive
Santa Monica, California 90406
Attention: Library — 1

Lockheed Missiles & Space Company
P.O. Box 504, Sunnyvale, California 94088
Attention: Library — 1

Mechanical Technology Incorporated
968 Albany-Shaker Road
Latham, New York 12110
Attention: Library — 2

North American Aviation, Inc.
Space and Information Systems Division
Downey, California 90241
Attention: Library — 1

Northern Research & Engineering Company
219 Vassar Street
Cambridge, Massachusetts 02139
Attention: Library — 1

Solar Division of International Harvester
2200 Pacific Highway
San Diego, California 92112
Attention: Library — 1

Space Technology Laboratories, Inc.
One Space Park
Redondo Beach, California 90278
Attention: Library — 1

Sunstrand Denver
2480 West 70th Avenue
Denver, Colorado 80221
Attention: Library — 1

Thompson-Ramo-Wooldridge Accessories Division
23555 Euclid Avenue
Cleveland, Ohio 44117
Attention: Library — 1

Union Carbide Corporation
Linde Division
P.O. Box 44, Tonawanda, New York 14152
Attention: Library — 1

United Aircraft Research Laboratory
East Hartford, Connecticut 06108
Attention: Library — 1

Westinghouse Electric Corporation
Astronuclear Laboratory
P.O. Box 10864, Pittsburgh, Pennsylvania 15236
Attention: Library — 1

Williams Research
Walled Lake, Michigan 48088
Attention: Library — 1